Heating Structures Derived from Satellite

W.-K. Tao[1], R. Adler[1], Z. Haddad[2], A. Hou[1], R. Kakar[3], T. N. Krishnamurti[4], C. Kummerow[5], S. Lang[6], R. Meneghini[1], W. Olson[7], S. Satoh[8], S. Shige[8], J. Simpson[1], E. Smith[1], Y. Takayabu[9], and S. Yang[10]

[1]*NASA/Goddard Space Flight Center*

[2]*NASA/JPL*

[3]*NASA/HQ*

[4]*Florida State University*

[5]*Colorado State University*

[6]*Science Systems and Applications Inc.*

[7]*Joint Center for Earth Systems Technology*
University of Maryland, Baltimore County
Baltimore, MD

[8]*Japan Aerospace Exploration Agency (JAXA)*

[9]*CCSR/U. of Tokyo*

[10]*George Mason University*
Fairfax, VA

Bull. Amer. Meteor. Soc.

(December 18 2003)

Corresponding author address: Dr. Wei-Kuo Tao, Mesoscale Atmospheric Processes Branch, Code 912, NASA GSFC, Greenbelt, MD 20771
email: tao@agnes.gsfc.nasa.gov

Abstract

Rainfall is a key link in the hydrologic cycle and is a primary heat source for the atmosphere. The vertical distribution of latent-heat release, which is accompanied by rainfall, modulates the large-scale circulations of the tropics and in turn can impact midlatitude weather. This latent heat release is a consequence of phase changes between vapor, liquid, and solid water.

The Tropical Rainfall Measuring Mission (TRMM), a joint U.S./Japan space project, was launched in November 1997. It provides an accurate measurement of rainfall over the global tropics which can be used to estimate the four-dimensional structure of latent heating over the global tropics. The distributions of rainfall and inferred heating can be used to advance our understanding of the global energy and water cycle.

This paper describes several different algorithms for estimating latent heating using TRMM observations. The strengths and weaknesses of each algorithm as well as the heating products are also discussed. The validation of heating products will be exhibited. Finally, the application of this heating information to global circulation and climate models is presented.

Heating Structures Derived from Satellite

W.-K. Tao, R. Adler, Z. Haddad, A. Hou, R. Kakar, T. N. Krishnamurti, C. Kummerow, S. Lang, R. Meneghini, W. Olson, S. Satoh, S. Shige, J. Simpson, E. Smith, Y. Takayabu, and S. Yang

Submitted to ***Bulletin of the American Meteorological Spciety***

Popular Summary

Rainfall is a key link in the hydrologic cycle and is a primary heat source for the atmosphere. The vertical distribution of latent-heat release, which is accompanied by rainfall, modulates the large-scale circulations of the tropics and in turn can impact midlatitude weather. This latent heat release is a consequence of phase changes between vapor, liquid, and solid water.

The Tropical Rainfall Measuring Mission (TRMM), a joint U.S./Japan space project, was launched in November 1997. It provides an accurate measurement of rainfall over the global tropics which can be used to estimate the four-dimensional structure of latent heating over the global tropics. The distributions of rainfall and inferred heating can be used to advance our understanding of the global energy and water cycle.

This paper describes several different algorithms for estimating latent heating using TRMM observations. The strengths and weaknesses of each algorithm as well as the heating products are also discussed. The validation of heating products will be exhibited. Finally, the application of this heating information to global circulation and climate models is presented.

1. Introduction

The global hydrological cycle is central to climate system interactions and the key to understanding their behavior. Rainfall and its associated precipitation processes are a key link in the hydrologic cycle. Fresh water provided by tropical rainfall and its variability can exert a large impact upon the structure of the upper ocean layer. In addition, almost two-thirds of the global rainfall occurs in the tropics[1]. Precipitation from convective cloud systems comprises a large portion of tropical rainfall and associated heating. Furthermore, the vertical distribution of convective and stratiform latent-heat release modulates large-scale tropical circulations and climates (Hartmann *et al.* 1984; Lau and Peng 1987; Sui and Lau 1988; Schumacher *et al.* 2003). The Tropical Rainfall Measuring Mission (TRMM), a joint U.S./Japan project, is a satellite mission intended to provide an adequate measurement of rainfall as well as an estimation of the four-dimensional structure of diabatic heating over the global tropics using an inclined low-altitude orbit and the combination of a precipitation radar (PR), a visible infrared scanner (VIRS) and the TRMM microwave imager (TMI) (see Simpson *et al.* 1988, 1996). The distributions of rainfall and inferred heating can be used to advance our understanding of the global energy and water cycle. In addition, TRMM data can be used for global circulation and climate models for testing and improving their parameterizations.

Latent heating is the heat released or absorbed by the atmosphere as a result of phase changes in water (i.e., gas to liquid, liquid to solid, gas to solid or vice versa). It is dominated by phase changes between water vapor and small, cloud-sized particles, which cannot be directly detected with TRMM sensors. Cloud-resolving models (CRMs), however, can simulate the phase changes in water and

---

1 The Tropics is loosely defined as the longitudinal belt from 25 N to 25 S.

the conversion of water species explicitly (i.e., Soong and Tao 1980; Tao and Soong 1986; Tao *et al.* 1993a, and many others). For example, (1) shows the thermodynamic (or temperature budget) that can be explicitly calculated from CRMs.

$$Q_1 - Q_R = \bar{\pi}[-\frac{1}{\bar{\rho}}\frac{\partial \bar{\rho} w'\theta'}{\partial z} - V' \bullet \nabla\theta'] + \frac{L_v}{C_P}(c-e) + \frac{L_f}{C_P}(f-m) + \frac{L_s}{C_P}(d-s) \qquad (1)$$

The primes indicate deviations from large-scale environment (cloud or small scale). The variable θ is the potential temperature, $\bar{\rho}$ is the density, and $\bar{\pi} = (p/P_{oo})^{R/Cp}$ is the nondimensional pressure, where P is the dimensional pressure and p_{oo} the reference pressure taken to be 1000 mb. C_p is the specific heat of dry air at constant pressure, and R is the gas constant for dry air. The variables L_v, L_f and L_s are the latent heats of condensation, fusion and sublimation, respectively. The variables *c*, *e*, *f*, *m*, *d* and *s* stand for the rates of condensation, evaporation of cloud droplets and raindrops, freezing of raindrops, melting of snow and graupel, deposition of ice particles and sublimation of ice particles, respectively. The term Q_1 is the apparent heat source (Yanai *et al.* 1973) and Q_R is the cooling/heating rate associated with radiative processes. Also, the first two terms on the right-hand side of (1) is the horizontal and vertical eddy heat convergence. The horiozntal eddy heat convergence can be neglected when the (1) is averaged horizontally over a large area (Yanai *et al.* 1973).

Figure 1 shows the instantaneous latent heating structure associated with a tropical and a midlatitude mesoscale convective system (MCS) simulated by a 2D CRM, the Goddard Cumulus Ensemble (GCE) model. Generally, there are many similarities in the latent heating structure between these two cases. These include (condensation) heating in the lower to middle troposphere in the convective leading edge of the cloud system. Deposition heating occurs in the upper part of the

convective region and in the upper part of the stratiform region. The cooling at low levels in the stratiform region is from the evaporation of rain. Cooling from melting of precipitation particles can also contribute to latent heating and mainly occurs in a narrow layer near the freezing level (Tao *et al.* 1993b). There is cooling from sublimation adjacent to depositional heating in the stratiform region. The heating/cooling pattern is mainly caused by gravity waves induced by the deep convection. This feature is more significant in the midlatitude case because the midlatitude convective updrafts are stronger. There are also some major differences between these cases, however. For example, the cooling from the stratiform region is larger and thicker for the midlatitude case than the tropical case. This is due to the drier, midlatitude environment. In addition, the level separating the heating and cooling in the stratiform region (indicating the freezing or melting level) is different for these two convective systems.

Latent heating profiles and the vertical eddy heat convergence can be derived indirectly by measuring the vertical profiles of temperature and the three-dimensional wind fields from extensive rawinsonde networks through a residual method as shown in (2) (called a diagnostic budget; Yanai *et al.* 1973; Houze 1982, 1989, 1997; and Johnson 1984). Heating profiles for the TRMM field campaign sites (i.e., SCSMEX, May - June 1998; LBA - TRMM/Brazil, January - February 1999; and KWAJEX, July - September 1999[2]) as well as other major field campaigns such as

---

[2] South China Sea Monsoon Experiment (SCSMEX), May - June 1998; Large Scale Biosphere-Atmosphere Experiment in Amazonia, (LBA) - TRMM/Brazil, January - February 1999; and Kwajalein Experiment. (KWAJEX), July - September 1999. DOE/ARM stands for Department of Energy Atmospheric Radiation Measurement

DOE/ARM can be used for validation. Q_1 can be calculated either from grid values in a large- or regional-scale prediction model or from large-scale re-analyses (Nigam *et al.* 2000).

$$Q_1 - Q_R = \overline{\pi}[\frac{\partial \overline{\theta}}{\partial t} + \overline{V} \bullet \nabla \overline{\theta} + \overline{w}\frac{\partial \overline{\theta}}{\partial z}] \qquad (2)$$

In section 2, the latent heating algorithms developed for TRMM will be discussed. The strengths and weaknesses of each algorithm will also be shown. Highlights from these algorithms will be presented and discussed in section 3. Validation of the heating algorithms will be presented in section 4. Future work and the application of the heating products will be discussed in section 5.

2. How can latent heating be derived?

Time series of the apparent heat source Q_1 diagnostically determined by soundings and explicitly calculated by the GCE model for the period 19-26 December 1992 are illustrated in Figs. 2(a) and (b). The pattern of temporal variability between the heating profiles derived from the soundings and estimated by the GCE model agree quite well. This is because that the large-scale advective forcing in temperature and water was superimposed into the GCE model as the main forcing (Soong and Tao 1980; Tao and Soong 1986). The latent heat release associated with all five major rainfall events are well simulated by the GCE model. Model results, however, show more temporal variability. This is perhaps caused by the fact that diagnostically determined Q_1 was calculated using 6-hourly soundings and a 1-2-1 filter was applied (Lin and Johnson 1996). The GCE model estimates are based on 2 minute statistics of cloud processes (i.e., condensation, evaporation, deposition, sublimation, freezing and melting rates) without any smoothing. This result clearly indicates that

CRMs can provide cloud data sets associated with various types of clouds and cloud systems from different geographic locations for the TRMM retrieval algorithm database [see review by Tao *et al.* (2000, 2001)]. The data represent instantaneous values and are selected from periods where the cloud and precipitation fields meet predetermined characteristics that are unique or complementary to the database requirements.

Five different latent heating algorithms, the Goddard Convective-Stratiform Heating (CSH), the Goddard Profiling (GPROF) heating, the Hydrometeor Heating (HH), the Spectral Latent Heating (SLH) and the Precipitation Radar Heating (PRH) algorithm have been developed to retrieve latent heating profiles using TRMM rainfall products. The HH algorithm estimates the latent heating profiles of clouds/cloud systems as a function of the vertical derivative of their retrieved hydrometeor profiles termed a *hydrometeor/heating (HH)* algorithm (Tao *et al.* 1990, 1993b; Yang and Smith 1999 a,b,2000). The derivation and evaluation of the HH algorithm was based on CRM simulations, and it requires information about the vertical profiles of cloud- and precipitation-sized water and ice particles, all of which can be obtained from the TMI retrievals (Kummerow *et al.* 1996; Smith *et al.* 1992, 1994). The terminal (fall) velocities of the large cloud (precipitating) particles (rain, snow and graupel/hail) are also required for the HH algorithm. Empirical coefficients associated with the condensation of small liquid water droplets and deposition of small ice particles are needed in Tao *et al.* (1990). These coefficients can also be determined using the surface rain rates (Tao *et al.* 1993b). Cloud-scale velocity is needed in the HH algorithm developed by Yang and Smith (1999a). It is obtained by applying a regression method to a CRM-simulated data base.

The second method, the CSH algorithm, only needs information on surface precipitation rates, fraction of stratiform rain, and the type and location of observed cloud systems (Tao *et al.* 1993b). A lookup table however, is needed containing stored convective and stratiform latent heating profiles, normalized by total surface rain rates, for various types of cloud systems in different geographic locations. These profiles are mostly obtained from CRM (GCE model) simulations. In the third method, the GPROF, CRM-simulated hydrometeor/latent heating vertical profiles that have radiative characteristics consistent with a given set of multi-spectral, microwave, radiometric observations are composited to create (retrieve) a best estimate of the observed profiles (Olson *et al.* 1999).

The SLH algorithm (Shige *et al.* 2003) is also a table method based on GCE model results. But its uniqueness resides in the fact that it utilizes spectral latent heating tables based on precipitation top heights or melting-level rain rates, for convective rain and for stratiform rain, respectively The PRH algorithm (Satoh and Noda 2001) also uses PR information but without using any heating profiles simulated by CRMs. However, it needs to estimate the cloud drafts and (standard) thermodynamic structures associated with cloud systems. An iteration calculation is applied to match the relationship between rainfall and latent heating. Table 1 summarizes the information required by each algorithm and lists some of the cases to which they have been applied in previous latent heating retrieval studies.

The CSH, SLH, and GPROF algorithms can estimate the latent heating [microphysics processes shown in (1)] Q_1-Q_R, and /or Q_1 because they use the cloud data generated from CRMs. The CRMs can provide cloud data bases consisting of either latent heating or Q_1-Q_R explicitly. The HH and PRH algorithms can only estimate the latent heating profiles.

A quantitative comparison between three of the heating algorithms (CSH, GPROF and HH) was performed (Tao *et al.* 2001). The results indicated that the horizontal distribution or patterns of latent heat release retrieved by these three different methods are quite similar and highly relate to the surface rainfall. They can all identify the areas of major convective activity [i.e., a well defined Intertropical Convergence Zone (ITCZ) in the Pacific and a distinct South Pacific Convergence Zone (SPCZ)]. The magnitude of their estimated latent heat release is also in good agreement with each other and with those determined from diagnostic budget studies. The major difference between these three heating retrieval algorithms is in the altitude of the maximum heating level. The CSH algorithm-estimated heating profiles only show one maximum heating level, and the level varies between various geographic locations. These features are in good agreement with diagnostic budget studies. A broader heating maximum, often with two embedded peaks, is generally obtained by the GPROF and HH algorithms, and the response of the heating profiles to variations in convective activity is less pronounced. Also, GPROF and HH generally yield heating profiles with a maximum at somewhat lower altitudes than those from the CSH. The strengths and weakness of these heating algorithms are listed in Table 2.

3. Heating structures estimated from various heating algorithms

3.1 Instantaneous latent heating structure

Figure 3 shows the algorithm-derived surface rain rates, convective rain rates, total precipitation and $Q_1 - Q_R$ estimated from TMI (GPROF) observations of a squall line in the tropical North Atlantic. The heaviest rains are seen along the convective

leading edge of the system, while generally lower rain intensities are observed in the trailing stratiform areas to the north and west of the leading edge. The cross section [Fig. 3(c)] is nearly perpendicular to the leading edge, crossing not only the stratiform rain behind the line but also what appears to be decaying convection further rearward. The leading-edge convection is characterized by relatively high water contents, exceeding 1 g m^{-3} near the surface. Horizontally collocated with the maximum rain water contents are the maximum estimated heating rates, which exceed 9 K h^{-1} between 5 and 8 km latitude. A secondary heating peak associated with possible decaying convection is seen near the 80 km mark. Also, the maximum cooling (3 K h^{-1}) is located beneath this secondary heating peak. The overall heating structure is similar to those shown in Fig. (1) except that very fine features simulated by the GCE model cannot be captured by TRMM due to the coarser resolution of the TMI.

Figure 4 shows surface rain rates and latent heating for hurricane Bonnie from the HH algorithm which is based on the vertical derivative of rain mass flux from the combined TMI/PR rain retrieval algorithm. The early version of this combined (TMI/PR) algorithm has been described in detail by *Ziad et al.* (1997). A Legendre Polynomial (LP) function is introduced to smooth unrealistic spikes or noise in the retrieved rain profiles so that HH provides the general characteristics of the latent heating structure. The structure of the hurricane eye and the convective rain spiral bands are well captured. Rain rates appear at very high altitudes where deep convection exists, such as around 200km along the track [Fig. 4(b)]. There are lots of weak raining areas located in between the convective cells. In these weak precipitation areas, rain rates are mostly concentrated in the middle to lower troposphere, where stratiform conditions likely exist. Large latent heating profiles are always associated with the strongest deep convective cells [Fig. 4(c)]. The peaks

of maximum latent heating vary with different conditions. For example, the peak is located at 3-5 km at 180km along the track, while it is at 3-4 km at 200km along the track. The heights of latent heating maximum seem mostly to be at and below 5 km. Cooling occurs in the lower troposphere in these stratiform regions. Overall, the general structure of latent heating based on the HH algorithm appears reasonable for the hurricane Bonnie case. However, it should be pointed out that the height of maximum latent heating is lower than that from published large-scale heating budget studies for strong storms and from previous retrieved latent heating profiles. This conclusion is expected because the current combined TMI/PR rain retrieval algorithm does not retrieve solid hydrometeor profiles. Thus, a portion of the latent heating from phase changes of these hydrometeors is missing from the current HH algorithm output. This issue will be corrected in the next version.

Figure 5 shows the latent heating profiles associated with a typhoon at its developing stage retrieved by the SLH and PRH algorithm. The PR-estimated rain rates that are used as the input for these heating algorithms are also shown in Fig. 5. Overall, there are many similarities between the SLH- and PRH-retrieved latent heating profiles. For example, strong heating is retrieved from these two algorithms on both sides of the eyewall. The strong heating is very narrow in the lower troposhere on the right side of the eyewall. Away from the eyewall, the heating pattern is quite similar to that observed and simulated by CRMs in the stratiform region of mesoscale convective systems (Houze 1982, 1997; Tao *et al.* 1993b, 2000; Lang *et al.* 2003). However, there are also some major differences between the two algorithm-retrieved heating profiles. For example, the SLH algorithm-retrieved maximum heating level is lower than for the PRH algorithm [i.e., Fig. 5(d) and (e)]. The cooling retrieved by the PRH algorithm in the lower troposphere is stronger than that for the SLH algorithm. In addition, finer and

more detailed heating structures are retrieved by the PRH algorithm. The general structure between the SLH-retrieved Q_1 - Q_R and latent heating profile is similar except that the Q_1 - Q_R profile has higher and stronger maximum heating level [Fig. (5(e)].

Figure 6 shows the latent heating profiles associated with a mesoscale convective system over the tropical ocean northwest of Australia retrieved by the SLH and PRH algorithm. The PR-estimated rain rates that are used as the input for the SLH algorithm are also shown in Fig. 6. Strong heating (>10 K h^{-1}) is always associated with large rain rates (> 50 mm h^{-1}) in the convective region of the squall system. There is weak heating aloft and cooling below in the trailing stratiform region. The SLH algorithm can estimate both latent heating and Q_1 - Q_R. Both Q_1 - Q_R and latent heating averaged profiles peak at middle levels [about 6.0 km and see Fig. 6(d)]. This is in good agreement with having a heating maximum in the midtroposphere for Australian Monsoon Experiment (AMEX) convective systems (Frank and McBridge 1989). The estimated latent heating profile has a distinct cooling near 4.0 km, which is due to the melting processes. On the other hand, the estimated Q_1 - Q_R profile does not have this cooling near 4.0 km. This is because the eddy heat flux convergence compensates the distinct cooling due to the melting (i.e., Tao *et al.* 2003). As the typhoon case, the PRH-estimated heating has very fine structure and shows stonger cooling in the lower troposphere compared to the SLH-estimated.

Latent heating profiles for a midlatitude squall line retrieved by the PRH algorithm are shown in Fig. 7. The PR-observed radar reflectivity and estimated rainrate used as inputs into the PRH algorithm are also shown in Fig. 7. The radar reflectivity is very similar to that in an observed PRESTORM squall line (Rutledge *et*

al. 1988). Strong heating (>10 K h^{-1}) is always associated with large rain rates (> 50 mm h-1) at the leading edge of the squall system. There is weak heating aloft and cooling below in the trailing stratiform region. These features are very similar to those simulated by CRMs [i.e., Fig. 1(b), Lang *et al.* 2003], observed (Johnson and Hamilton 1988) and retrieved by the GPROF algorithm [Fig. 3(c)]. The total heating shown in Fig. 7(d) is also quite similar simulated by CRM and observed.

The heating profiles retrieved by these different heating algorithms qualitatively agree with each other for a squall line (PRH and GPROF), a typhoon/hurricane (SLH, PRH and HH) and a tropial oceanic MCS but not quantiatively. For example, the PRH-estimated heating has very fine structure and shows stonger cooling in the lower troposphere compared to the SLH-estimated. Some of the differences are caused by the different resolutions used in these algorithms. The assumptions used in different algorithms can also cause the difference. A thorough and detailed comparison is under way.

3.2 *Temporal and spatial averages*

Figures 8(a), (b) and (c) show five-yearly mean latent heating at three different altitudes (2, 5 and 8 km) over the global tropics from the CSH algorithm using PR-based rainfall products. The horizontal distribution of the CSH-estimated Q_1 structures is very similar to the pattern of surface rainfall [Fig. 8(d)], especially at middle and upper levels. For example, a well defined ITCZ in the east and central Pacific and in the Atlantic Ocean, the SPCZ, and broad areas of precipitation events spread over the continental regions are present. Also, strong latent heat release (5 K day^{-1} or greater) in the middle and upper troposphere is always associated with heavier surface precipitation. Heating in the upper troposphere over the Pacific and

Indian Oceans covers a much broader area than the heating over Africa, S. America and the Atlantic Ocean. The differential heating distribution between land and ocean in the upper troposphere could generate strong horizontal gradients in the thermodynamic fields and interact with the global circulation.

One interesting result from Fig. 8 is the relatively weak heating and cooling (-1 to 1 C day^{-1}) at the 2 km level over the Pacific Ocean. This result may be due to the fact that the moisture content is high over the Pacific ocean. Cooling by evaporation of raindrops in the lower troposphere could be weak over moist areas. Another possibility is that the convective heating and the stratiform cooling in the lower troposphere cancel each other.

Figure 9 shows the vertical average Q_1 profiles for spring, summer, fall and winter over the global tropics, land, and oceans. Globally, the summer and fall seasons show stronger heating associated with larger and heavier rainfall. Over land, the summer season has the strongest heating. Heating during the spring and fall seasons is quite similar. A cooling at lower troposphere occurs over land but not over ocean. The heating pattern (maximum heating level and its magnitude) over oceans is very similar to the global average. This is due to the fact that 70% of the tropics is covered by ocean.

The Q_1 structure associated with two climate events, an El Nino (December 1997 through February 1998) and a La Nina (December 1998 through February 1999) are examined. Figures 10(a) and (b) show the retrieved heating anomalies for these two climate events. The results show the largest signal over the equatorial Pacific, west Pacific and Indian ocean. The Q_1 pattern over the maritime continent, America and Africa is quite similar. Time (monthly) series of latent heating profiles

over the tropics and their deviations (from the mean) are shown in Fig. 10(c). The level of maximum heating is at 7.5 km. The variation of the maximum heating level as well as the magnitude are quite small. This is caused by the fact that the global tropical rainfall for El Nino (2.35 mm day^{-1}) and La Nina (2.40 mm day-^{1}) is quite similar as observed by the PR. However, there are cold and warm anomalies during El Nino and La Nina periods. These features are due to the fact that the PR observed a higher percentage of stratiform precipitation during the El Nino which is conducive to retrieving stronger low-level cooling compared to the La Nina.

4. How can latent heating be validated?

4.1 Validation with CRMs - a consistency check

Consistency checks were performed by several CRM-generated cloud data base heating algorithms (i.e., the CSH and SLH algorithms). The procedure is to use CRM-simulated parameters [i.e., surface rain rate, stratiform percentage, rain rate at the melting level, and precipitation top height (PTH)] to re-construct (or retrieve) heating profiles and compare them to sounding estimates and/or the CRM simulation. The TOGA COARE IFA region for the 16-26 December 1992 period (shown in Figure 2) was used for a consistency check for both the CSH and SLH algorithms. Other TOGA COARE periods, GATE[3] and DOE/ARM periods were also used for consistency checks (Tao *et al.* 2000; Shige *et al.* 2003).

---

3 GATE stands for GARP (Global Atmospheric Research Program) Atlantic Tropical Experiment

Figure 11 shows the time series of the CSH-retrived Q_1 averaged over the TOGA COARE IFA region. The results indicate the CSH-retrieved Q_1 profiles[4] are in very good agreement with those determined diagnostically by sounding as well as simulated by the GCE model (Fig 2). It is perhaps not too surprising because the heating profiles based on the GCE model-simulated rainfall rates and stratiform amounts are in very good agreement with those diagnostically determined. The GCE model is driven by the large-scale advective forcing in temperature and water vapor, and therefore the model's simulated rainfall and stratiform amount is simply a response to the forcing (Soong and Tao 1980). But, using the output from the GCE model for the CSH heating algorithm does not assure a good Q_1 retrieval. For example, errors in the estimated amount of stratiform rainfall can retrieve maximum heating at the wrong height.

Figure 12 shows the SLH algorithm-retrieved latent heating. The GCE model-simulated latent heating (not Q_1) is also shown in Fig. 12. Note that the difference between GE model simulated Q_1 and latent heating is quite small. This is because the latent heating term (20-40 K day^{-1}) is the dominant term in (1) compared to Q_R (1-2 K day^{-1}) and the vertical eddy heat convergence terms during active convective events (Soong and Tao 1980; Johnson *et al.* 2002). The temporal variations of the retrieved heating profiles agree well with that of the GCE-simulated heating profiles. In particular, the SLH (and CSH) algorithm-retrieved heating profiles captured the evolution of a quasi-2-day oscillation (Takayabu 2002) during the period 1800 UTC 23 - 1800 UTC 25 December 1992. The retrieved results

---

4 The heating profiles selected in the CSH algorithm's look-up table for this period are the GCE-modeled (6 hourly), time-averaged heating profiles from December 19 to 27, 1992.

have much smoother features [compared to Fig. 12(a)]. This is because the lookup tables represent the averaged profiles for each index, either PTH or precipitation rate at the melting level. Shige *et al.* (2003) also estimated the errors in the instantaneous heating structure at a grid point (1 km) spatial scale. The results show that spatial averaging (at least 50 km) is required to derive meaningful instantaneous heating profiles using the SLH algorithm.

4.2 Validation with sounding networks

Several field campaigns (SCSMEX, LBA and KWAJEX) conducted during 1998 and 1999 were aimed at the validation of TRMM products (i.e., rainfall and the vertical distribution of heating). Since latent heating profiles cannot be directly measured, CRMs are used in TRMM algorithms to provide a link between the latent heating profiles, and PR and TMI observations. Consequently, one of the key components of the TRMM field campaigns is to provide observations of the structure and evolution of MCSs, and individual convective clouds and their embedded large-scale environment. CRMs require these data sets for initial conditions as well as for the validation of their vertical latent heating structure.

Figure 13 shows a comparison between algorithm-retrieved heating and sounding estimates for SCSMEX during the most convectively active period (May 15 - June 20). Selecting the appropriate latent heating profiles from the CSH algorithm's look-up table for specific convective events is not a trivial problem. Two different approaches for selecting the latent heating profiles in the look-up table are used to obtain distinct estimates of the latent heating profiles in this comparison. *In the first approach,* normalized heating profiles representing oceanic conditions are obtained by averaging profiles from the look-up table based on a set of diagnostic

studies and the growing (but still limited) number of GCE model simulations (Figs. 3 and 4 in Tao *et al.* 2000). *In the second approach,* the heating profiles from look-up table profiles based on geographic locations and months of interest are utilized in the CSH algorithm (South China Sea for this comparison). In the SLH algorithm, the look-up table from the GCE SCSMEX simulation is selected.

The CSH algorithm-retrieved (Q_1) heating structures are stronger than sounding-estimated using the first approach. Nevertheless, there is some good agreement in the overall distribution (i.e., the maximum heating level using the heating profiles representing oceanic regions and cooling in the boundary layer). In contrast, the CSH algorithm-retrieved heating structures is in very good agreement with sounding estimated using the heating profiles from the GCE SCSMEX simulation. The maximum retrieved heating level is about 0.5 - 1 km lower than observed. The SLH algorithm-retrieved latent heating profile is in agreement both quantitatively and qualitatively with the sounding estimates' (Q_1) between the 2 and 5 km levels. The SLH algorithm-retrieved latent heating profile is stronger in the middle troposphere.

5. Future work

Heating profiles for the other TRMM field campaign sites as well as other major field campaigns such as DOE/ARM will be compared to profiles determined from the different heating algorithms. Dual-Doppler radar observations could also provide validation for algorithm-retrieved instantaneous heating profiles. This future comparison can provide an assessment of the absolute and relative errors of the heating retrieval algorithms. In addition, global analyses will be used to identify/compare the large-scale circulation patterns for the retrieved periods and

for periods during previous field campaigns (i.e., TOGA COARE and GATE). It is reasonable to assume that the latent heating structures for westerly wind bursts (WWBs) and super cloud clusters (SCCs) occurring in similar large-scale circulations and with similar SSTs may not be very different. An intercomparison between different heating algorithms (latent heating, Q_1, and/or Q_1-Q_R) is planned in 2004.

Since several heating algorithms require CRM-simulated cloud data sets including heating profiles (i.e., the lookup tables for the CSH and SLH algorithms, and rain rates and cloud profiles for GPROF), the number of heating profiles associated with different types of clouds and convective systems from various geographic locations needs to be increased. Data from TRMM field experiments and other major field experiments (i.e., DOE/ARM) can be used to provide initial conditions for CRMs and validate the CRM-simulated latent (diabatic) heating. The heating obtained from numerical model simulations and large-scale model re-analysis (Nigam *et al.* 2000) can be compared with those from retrieval algorithms. This comparison could identify what are the major physical processes that cause the similarities and differences between models. In addition, data from field campaigns can be used to validate and improve CRM microphysics because they are the major processes responsible for latent heat release.

The HH, GPROF, SLH and PRH algorithms can produce instantaneous heating profiles at the satellite foot print. The assumption is that instantaneous heating profiles and cloud/rain structures are related. Shige *et al.* (2003) showed that spatial averaging (at least 50 km) is required to derive meaningful instantaneous heating profiles using the SLH algorithm. The key developers for the TRMM heating algorithms have agreed to examine the possibility of producing a unified

heating algorithm using microwave sensors (i.e., TMI/SSM-I[5]) and radar (i.e., PR) products for TRMM. It would require comparing the various heating algorithms using the same rainfall products as in Tao *et al.* (2001).

Two global climate models, from the NASA Goddard Space Flight Center (GSFC) and the Florida State University, are currently using TRMM data sets to either improve their cumulus parameterization schemes and/or identify the problems in these schemes. The direct use of satellite (and or other ground-based) products on heating profiles for atmospheric models requires a physical initialization design. For example, the Florida State University global, spectral model (Krishnamurti *et al.* 1991) has been developing a new cumulus parameterization scheme (NCPS) to use observed and/or satellite-retrieved heating profiles through an empirical approach. Since temperature (heating) and water vapor (moistening/drying) are closely related, a moisture profile is also needed in NCPS. The initial results with the NCPS incorporated into the FSU global spectral model shows improved precipitation and circulation (Rajendran *et al.* 2003) forecasts on day-2 and day-3 (Fig. 14). The use of satellite-derived profiles in data assimilation appears very promising but requires much further work. Particularly, there has to be closer cooperation between latent heating algorithm developers and the data assimilation/large-scale modeling communities. Research is currently underway at NASA GSFC to develop variational techniques to assimilate TMI-derived convective and stratiform latent heating rates within the general framework of parameter estimation using disposable parameters in moist physics schemes as a control variable. The aim is to explore the feasibility of improving global analyses and forecasts through the assimilation of CRM-based latent heating profiles that are radiatively compatible with multi-channel TMI brightness temperatures. The optimization of moist physics parameterizations in the

---

5 SSM/I stands for Special Sensor Microwave/Imager.

context of data assimilation can provide valuable information for diagnosing model deficiencies and guiding the improvement of parameterization schemes.

There is another major application using NWP and/or global circulation models with satellite-retrieved heating profiles. As the number of such models subjected to initialization by the different observed/retrieved heating profiles increases major improvements in forecasting capabilities via ensemble or superensemble (Krishnamurti *et al.* 2001) techniques can be expected. This is being established as a powerful technique. The goal is to reduce overall uncertainties as well as to better estimate errors associated with models, data sets and parameterizations.

6. Acknowledgement

This study is supported by the U. S. NASA and Japan Aerospace Exploration Agency (JAXA) TRMM project.

7. References

Frank, W. M. and J. L. McBridge 1989: The vertical distribution of heating inAMEX and GATE cloud clusters. *J. Atmos. Sci.*, **46**, 3464-3478.

Hartmann, D. L., H. H. Hendon, R. A. Jr., Houze, 1984: Some implications of mesoscale circulations in tropical cloud clusters for large-scale dynamics and climate. *J. Atmos. Sci.*, **41**, 113-121.

Houze, R. A., Jr., 1982: Cloud clusters and large-scale vertical motions in the tropics. *J. Meteor. Soc. Japan,* **60,** 396-409.

Houze, R. A., Jr., 1989: Observed structure of mesoscale convective systems and implications for large-scale heating. *Quart. J. Roy. Meteor. Soc.,* **115,** 425-461.

Houze, R. A., Jr., 1997: Stratiform precipitation in regions of convection: A meteorological paradox. *Bull. Amer. Meteor. Soc.,* **78,** 2179-2196.

Johnson, D., W.-K. Tao, J. Simpson, and C.-H. Sui, 2002: A study of the response of deep tropical clouds to large-scale processes, Part I: Model set-up strategy and comparison with observation, *J. Atmos. Sci.,* **59,** 3492-3518.

Johnson, R. H., 1984: Partitioning tropical heat and moisture budgets into cumulus and mesoscale components: Implication for cumulus parameterization. *Mon. Wea. Rev.,* **112,** 1656-1665.

Johnson, R. H., and P. J. Hamilton, 1988: The relationship of surface pressure features to the precipitation and airflow structure of an intense midlatitude squall line. *Mon. Wea. Rev.,* **116,** 1444-1472.

Johnson, R. H., and P. E. Ciesielski, 2002: Characteristics of the 1998 summer monsoon onset over the Northern South China Sea. *J. Meteor. Soc. Japan,* **80,** 561-578.

Krishnamurti T. N., S. Surendran, D. W. Shin, R. J. Correa-Torres, T. S. Kumar, E. Williford, C. Kummerow, R. F. Adler, J. Simpson, R. Kakar, W. S. Olson and F. J.

Turk, 2001: Real-time multianalysis-multimodel superensemble forecasts of precipitation using TRMM and SSM/I products. *Mon. Wea. Rev.*, **129**, 2861-2883.

Krishnamurti T.N., J. S. Xue, H. S. Bedi, K. Ingles and D. Oosterhof, 1991: Physical Initialization for Numerical Weather Prediction Over the Tropics. *Tellus*, **43**, 53-81.

Kummerow, C., W. S. Olson, and L. Giglio, 1996: A simplified scheme for obtaining precipitation and vertical hydrometeor profiles from passive microwave sensors. *IEEE Trans. Geosci. Remote Sensing*, **34**, 1213-1232.

Lang, S., W.-K. Tao., J. Simpson, and B. Ferrier, 2003: Numerical modeling of Convective-stratiform precipitation processes: Sensitivity to partition methods. *J. Applied. Meteor.* **45**, 505-527.

Lau, K.-M., and L. Peng, 1987: Origin of low-frequency (intraseasonal) oscillations in the tropical atmosphere. Part I: Basic theory. *J. Atmos. Sci.*, **44**, 950-972.

Lin, X., and R. H. Johnson, 1996: Heating, moistening and rainfall over the western Pacific during TOGA COARE. *J. Atmos. Sci.*, 53, 3367-3383.

Nigam, S., C. Chung, and E. DeWeaver, 2000: ENSO diabatic heating in ECMWF and NCEP-NCAR reanalyses, and NCAR CCM3 simulation. *J. of Climate*, **13**, 3152-3171.

Olson, W. S., C. D. Kummerow, Y. Hong and W.-K. Tao, 1999: Atmospheric latent heating distributions in the Tropics derived from passive microwave radiometer measurements. *J. Appl. Meteor.*, **38**, 633-664.

Rajendran, R., T. N. Krishnamurti, V. Misra and W.-K. Tao, 2003: An empirical cumulus parameterization scheme based on TRMM latent heating profiles, *J. Meteor. Soc. Japan* (submitted).

Rutledge, S.A., R.A. Houze Jr., M.I. Biggerstaff, and T. Matejka, 1988: The Oklahoma-Kansas mesoscale convective system of 10-11 June 1985: Precipitation structure and single-doppler radar analysis. *Mon. Wea. Rev.*, **116**, 1409-1430.

Satoh, S. and A. Noda, 2001: Retrieval of latent heating profiles from TRMM radar data. Proceeding of 30th International Conf. On Radar Meteorology, Munich, Germany, 19-24 July 2001, 340-342.

Schumacher, C., R. A. Houze, Jr., and I. Kraucunas, 2003: The tropical dynamical response to latent heating estimates derived from the TRMM precipitation radar. J. Atmos. Sci., (accepted).

Shige, S., Y. N. Takayabu, W.-K. Tao and D. Johnson, 2003: Spectral retrieval of latent heating profiles from TRMM PR data. Part I: Development of a model-based algorithm. *J. Applied Meteor.* (accepted).

Simpson, J., R. F. Adler and G. R. North, 1988: A proposed tropical rainfall measuring mission (TRMM) satellite. *Bull. Amer. Meteor. Soc.*, **69**, 278-295.

Simpson, J., C. Kummerow, W.-K. Tao and R. Adler, 1996: On the Tropical Rainfall Measuring Mission (TRMM), *Phys. Meteor, and Atmos. Phys.* **60**, 19-36.Satoh, S. and A. Noda, 2001: Retrieval of latent heating profiles from TRMM radar data. Proceeding of 30th International Conf. On Radar Meteorology, Munich, Germany, 19-24 July 2001, 340-342.

Smith, E. A., X. Xiang, A. Mugnai and G. J. Tripoli, 1992: A cloud-radiation model algorithm for spaceborne precipitation retrieval. Extended Abstract Vol. of *International TRMM Workshop on the Processing and Utilization of the Rainfall Data Measured from Space*, Communications Research Laboratory, Tokyo, Japan, 273-283.

Smith, E.A., X. Xiang, A. Mugnai, and G.J. Tripoli, 1994: Design of an inversion-based precipitation profile retrieval algorithm using an explicit cloud model for initial guess microphysics. *Meteor. Atmos. Phys.*, 54, 53-78.

Soong, S.-T., and W.-K. Tao, 1980: Response of deep tropical clouds to mesoscale processes. *J. Atmos. Sci.*, **37**, 2016-2036.

Sui, C.-H. and K.-M. Lau, 1988: Origin of low-frequency (Intraseasonal) oscillations in the tropical atmosphere. Part II: Structure and propagation of mobile wave-CISK modes and their modification by lower boundary forcings. *J. Atmos. Sci.*, **46**, 37-56.

Takayabu, Y. N., 2002: Spectral representation of rain features and diurnal variations observed with TRMM PR over the equatorial areas. *Geophys. Res. Lett.*, **29**, 30-1-30-4.

Tao, W.-K., and S.-T. Soong, 1986: A study of the response of deep tropical clouds to mesoscale processes: Three-dimensional numerical experiments. *J. Atmos. Sci.*, 43, 2653-2676.

Tao, W.-K., J. Simpson, S. Lang, M. McCumber, R. Adler and R. Penc, 1990: An algorithm to estimate the heating budget from vertical hydrometeor profiles. *J. Appl. Meteor.*, **29**, 1232-1244.

Tao, W.-K., J. Simpson, C.-H. Sui, B. Ferrier, S. Lang, J. Scala, M.-D. Chou, and K. Pickering, 1993a: Heating, moisture and water budgets of tropical and mid-latitude squall lines: Comparisons and sensitivity to longwave radiation. *J. Atmos. Sci.*, **50**, 673-690.

Tao, W.-K., S. Lang, J. Simpson, and R. Adler, 1993b: Retrieval Algorithms for estimating the vertical profiles of latent heat release: Their applications for TRMM. *J. Meteor. Soc. Japan* , **71**, 685-700.

Tao, W.-K., J. Scala, B. Ferrier, and J. Simpson, 1995: The effects of melting processes on the development of a tropical and a mid-latitudes squall line. *J. Atmos. Sci.*, 52, 1934-1948.

Tao, W.-K., J. Simpson, S. Lang, C.-H. Sui, B. Ferrier, and M.-D. Chou, 1996: Mechanisms of cloud-radiation interaction in the tropics and midlatitudes. *J. Atmos. Sci* . 53, 2624-2651.

Tao, W.-K., S. Lang, J. Simpson, W. S. Olson, D. Johnson, B. Ferrier, C. Kummerow and R. Adler, 2000: Retrieving vertical profiles of latent heat release in TOGA COARE convective systems using a cloud resolving model, SSM/I and radar data, *J. Meteor. Soc. Japan*, **78**, 333-355.

Tao, W.-K., S. Lang, W. S. Olson, R. Meneghini, S. Yang, J. Simpson, C. Kummerow, E. Smith and J. Halverson, 2001: Retrieved vertical profiles of latent heat release using TRMM rainfall products for February 1998, *J. Appl. Meteor.*, **40**, 957-982.

Tao, W.-K., C.-L. Shie, R. Johnson, S. Braun, J. Simpson, and P. E. Ciesielski, 2003: Convective systems over the South China Sea: Cloud-resolving model simulations. *J. Atmos. Sci.*, (in press).

Wang, Y., W.-K. Tao and J. Simpson, 1996: The impact of ocean surface fluxes on a TOGA COARE cloud system. *Mon. Wea. Rev.*, 124, 2753-2763.

Yanai, M., S. Esbensen and J. Chu, 1973: Determination of average bulk properties of tropical cloud clusters from large-scale heat and moisture budgets *J. Atmos. Sci.*, **30**, 611-627.

Yang, S., and E. A. Smith, 1999a: Moisture budget analysis of TOGA-COARE area using SSM/I retrieved latent heating and large scale Q_2 estimates. *J. Atmospheric and Oceanic Technology*, **16**, 633-655.

Yang, S., and E. A. Smith, 1999b: Four Dimensional structure of monthly latent heating derived from SSM/I satellite measurements. *J. Climate*, **12**, 1016-1037.

Yang, S., and E. A. Smith, 2000: Vertical structure and transient behavior of convective-stratiform heating in TOGA-COARE from combined satellite-sounding analysis. *Journal of Applied Meteorology* , **39**, 1491-1513.

Haddad, Z.S., E.A. Smith, C.D. Kummerow, T. Iguchi, M.R. Farrar, s.L. Durden, M. Alves, and W.S. Olson, 1997: The TRMM 'Day-1'radar/radiometer combined rain-profile algorithm. J. Meteor. Soc. Japan, 75, 799-809.

TABLES

Figure Captions

Fig. 1: Latent heating (sum of heating by condensation, freezing and deposition, and sum of cooling by evaporation, melting, and sublimation) associated with **(a)** a midlatitude (PRESTORM) squall line and **(b)** a tropical (TOGA COARE) mesoscale convective system. These systems were simulated, and the results were presented in Tao *et al.* (1993a, 1995, 1996), Wang *et al.* (1996), and Lang *et al.* (2003). PRESTORM stands for Preliminary Regional Experiment for Storm Central, and TOGA COARE for Tropical Oceans Global Atmosphere (TOGA) - Coupled Ocean Atmosphere Response Experiment (COARE).

Fig. 2 Evolution of the apparent heating source (Q_1) averaged over the TOGA COARE (Intensive Flux Array) IFA for the 8-day period during December 19-27, 1992 **(a)** derived diagnostically from soundings (Lin and Johnson 1996) and **(b)** simulated from the GCE model.

Fig. 3 TMI-retrieved **(a)** surface rain rates, **(b)** convective rain rates, and **(c)** cross sections of total precipitation water content (shading) and Q_1 - Q_R (in K h^{-1}, contours) from GPROF from observations of a squall line in the North Atlantic on 7 April 1998. The horizontal resolution of the cross section is about 28 km.

Fig. 4 **(a)** TMI/PR retrieved near surface rain rate map for hurricane Bonnie (22 August 1998). **(b)** Cross section of rain rates and **(c)** HH algorithm-estimated latent heating profilesalong the track of the TRMM satellite at nadir from the precipitation radar.

Fig. 5 Cross section of **(a)** PR-estimated rain rate (in mm h^{-1}), **(b)** SLH-retrieved and **(c)** PRH-retrieved latent heating profiles (in K h^{-1}) associated with a tropical typhoon in the developing stage (2 August 2000). The arrow indicates the location of eye. The horizontal mean **(d)** SLH-retreved Q_1 - Q_R and latent heating profles and **(e)** PRH-retrieved latent heating profiles.

Fig. 6 Cross section of **(a)** PR-estimated rain rate (in mm h^{-1}), **(b)** SLH-retrieved and **(c)** PRH-retrieved latent heating profiles (in K h^{-1}) associated with a MCS over Australia. **(d)** is the horizontal mean SLH-retrieved latent heating and Q_1 - Q_R. and **(e)** the PRH-retrieved latent heating profiles.

Fig. 7 Cross section of **(a)** PR-observed radar reflectivity (ZE in dBZ), **(b)** PR estimated rain rate (in mm h^{-1}) and **(c)** PRH-retrieved latent heating profiles associated with a midlatitude (Oklahoma) squall line (10 May 1999). **(d)** is the horizontal mean PRH-retrieved latent heating profiles.

Fig. 8 Five-yearly mean Q_1 profiles at **(a)** 8, **(b)** 5 and **(c)** 2 km (above ground level, AGL) over the global tropics. Heating profiles representing just tropical oceanic and general land regions from the CSH look-up table (LUT) are used.

Fig. 9 Vertical average heating profiles for spring, summer, fall and winter over **(a)** the global tropics, **(b)** land, and **(c)** oceans.

Fig. 10 Retrieved heating anomalies for El Nino during DJF 1997-8 **(a)** and La Nina during December. January and February (DJF) 1998-9 **(b)** using

TRMM PR data and the Goddard Convective and stratiform heatin (CSH) algorithm at 8 km AGL. **(c)** shows the average heating profiles over the global tropics.

Fig. 11 Time series of CSH-retrieved Q_1 profiles averaged over the TOGA COARE IFA for the 8-day period during December 19-27, 1992. The GCE model-simulated rainfall rates and stratiform percentages are used. Contours are every 5 K day^{-1}.

Fig. 12 Time series of **(a)** GCE model simulated and **(b)** SLH algorithm-retrieved latent heating profiles averaged over the TOGA COARE IFA for the 8-day period during December 19-27, 1992. The GCE-simulated precipitation path top, convective/stratiform characteristics, precipitation rate at the melting level, and precipitation rate at the surface. These retrieved heating profiles are averaged over the GCE model domain (512 km in the horizontal). Contours are every 5 K day^{-1}.

Fig. 13 Heating from observations and retrieved from the CSH and SLH algorithms for SCSMEX from 15 May to 20 June 1998. Two sets of look-up-table profiles, one representing general tropical oceanic regions and another representing the South China Sea region, from the CSH algorithm were used for comparison. The observed, sounding-estimated profile comes from Johnson and Ciesielski (2002).

Fig. 14 Precipitation for 8 February 1998 from **(a) the** Global Precipitation Comparison Project (GPCP, observation), **(b)** the Florida State University

global spectral model (FSUGSM) day-2 forecast with NCPS, and **(c)** the FSUGSM control day-2 forecast. From Rajendran *et al.* (2003).

	Input	Cases	Resolution
Tao *et al.* (1991) HH Algorithm	Surface Rainfall, Hydrometeor Profiles (cloud water, rain, cloud ice, snow and graupel) and Terminal velocity of rain, snow and graupel	GATE (1974), PRESTORM (1985)	200 - 300 km daily
Tao *et al.* (1993) CSH Algorithm	Surface Rainfall and its stratiform percentage	GATE (1974), PRESTORM (1985), Typhoon Thelma (1987)	200 - 300 km daily
Olson *et al.* (1999) GPROF	Cloud modeled latent heating profiles and hydrometeor profiles	Hurricane Andrew (1992), TOGA COARE (1992-93)	25 - 50 km Instantaneously
Yang and Smith (1999a, b, 2000) HH Algorithm	Hydrometeor Profiles (cloud water, rain, ice particles) and Cloud Vertical Velocities/ Terminal Velocity of rain and ice particles	TOGA COARE (1992-93) Global Tropical region (1992)	15 - 50 km Instantaneously 2.5° x 2.5° Monthly
Tao *et al.* (2000) CSH Algorithm	Surface Rainfall and its stratiform percentage	TOGA COARE (1992-93)	500 x 500 km 3-6 hourly
Tao *et al.* (2001)	**CSH, GPROF and HH Algorithms**	February 1998	1° x 1° Daily
Shige *et al.* (2003) SLH Algorithm	Convective and stratiform Characteristics Precipitation Top Height Rainfall rate at melting layer	TOGA COARE (1992-93)	500 x 500 km 3-6 hourly
Tao *et al.* (2003)	**SLH-PRH, HH, GPROF, CSH Algorithms**	Major convective event (i.e., hurricane), global tropical, validation sites	Instantaneously 2.5° x 2.5° Monthly

Table 1

Algorithm	Strengths	Weakness
Convective and Stratiform (Tao *et al.* 1993, 2000, 2001, 2002)	Based on (convective/stratiform) heating characteristics derived from diagnostic budget study Validated with 1992-1993 TOGA COARE, LBA, KWAJEX, SCSMEX data Produced one single maximum heating level for Feb 1998 – Good agreement with observations	Sensitive to stratiform amount Sensitive to the heating profiles stored in the CSH look-up table No rainfall -> no latent heating aloft
GPROF (Olson *et al.* 1999)	Method is physically-based; latent heating profiles are consistent with other retrieved parameters. Random error of retrieved parameters can be estimated using Bayesian approach. Latent heating profiles are retrieved at footprint resolution (~10 km); may be "verified" using coincident dual-doppler radar observations.	Rainfall and latent heating may have different temporal scale. Errors in cloud/radiative model simulations can lead to biases in retrieved heating profiles. Under-representation of observed precipitation and latent heating structures in cloud/radiative model database can lead to errors in estimates.
HH (Yang *et al.* 1999a,b, 2000; Tao *et al.* 1990, 1993)	Physical approach --- Latent heating is closely related to the reality of atmosphere if retrieved hydrometeor profiles are accurate Both pixel and area mean resolutions Ready to use --- Could be easily adapted to 2A-12, 2B-31 outputs to estimate latent heating	Sensitive to accuracy of retrieved hydrometeor profiles --- Any error from hydrometeor profiles will be passed to latent heating profiles Uncertainty with cloud scale atmosphere vertical motion (assumed W=0 if W is unknown) Uncertainty in identifying melting layer Uncertainty in estimating terminal velocity of particles
SLH (Shige *et al.* 2003)	Produces realistic heating profiles for various cloud system regimes (e.g. shallow and deep convective regimes) - PTH Produces heating profiles for decaying MCSs even with no surface rain - RRmelt Heating profiles are retrieved at foot print resolution (4km)	Sensitive to the heating profiles generated from cloud-resolving model Low sampling rate due to the narrow swath width of PR (spatial averaging is needed)
PRH (Satoh and Noda 2001)	Produces realistic heating profiles for various cloud systems (e.g. squall lines, typhoons) Does not depend on cloud-model-simulated heating profiles	Sensitive to the estimated air velocity and hydrometeor profiles (especially in the mixed phase) Produces cooling near cloud top and in the upper parts of clouds sometimes Low sampling rate due to the narrow swath width of the PR

Table 2

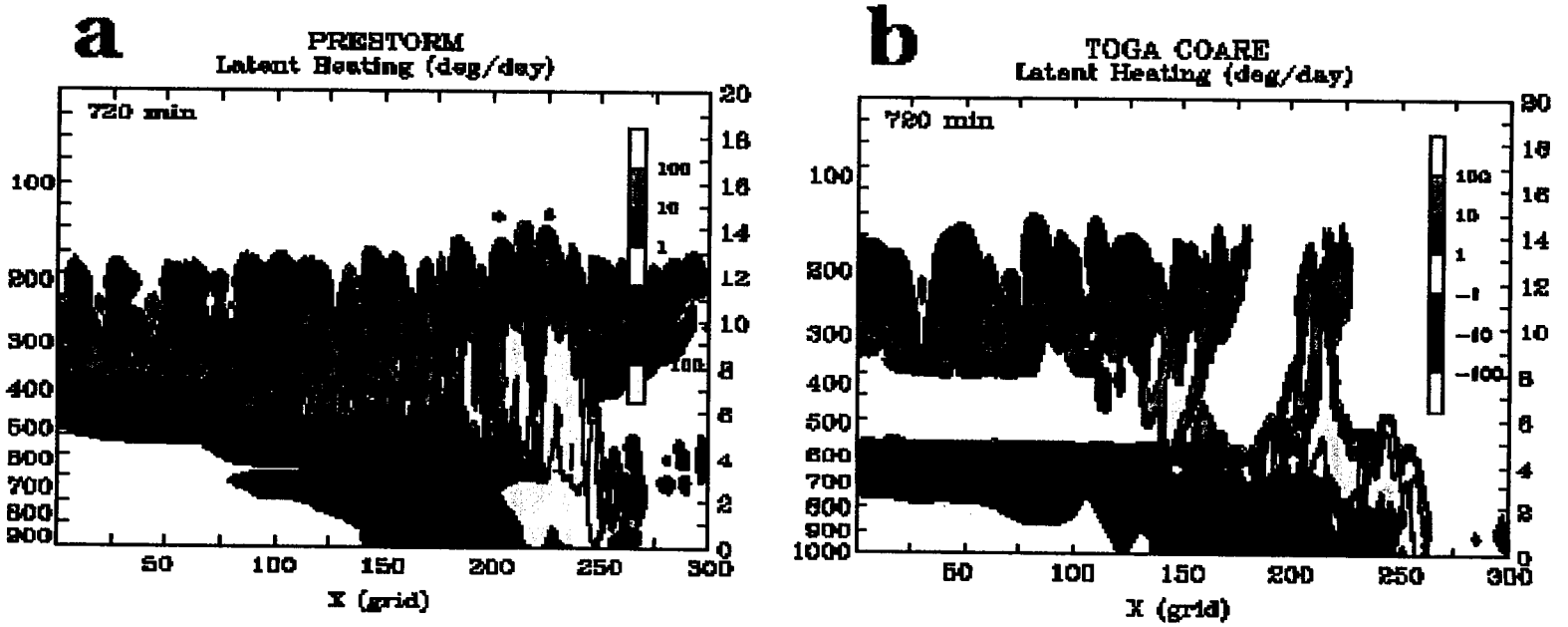
a
PRESTORM
Latent Heating (deg/day)
720 min
100
200
300
400
500
600
700
800
900
20
18
16
14
12
10
8
6
4
2
0
50
100
150
200
250
300
X (grid)
b
TOGA COARE
Latent Heating (deg/day)
720 min
100
200
300
400
500
600
700
800
900
1000
20
18
16
14
12
10
8
6
4
2
0
50
100
150
200
250
300
X (grid)

Fig. 1

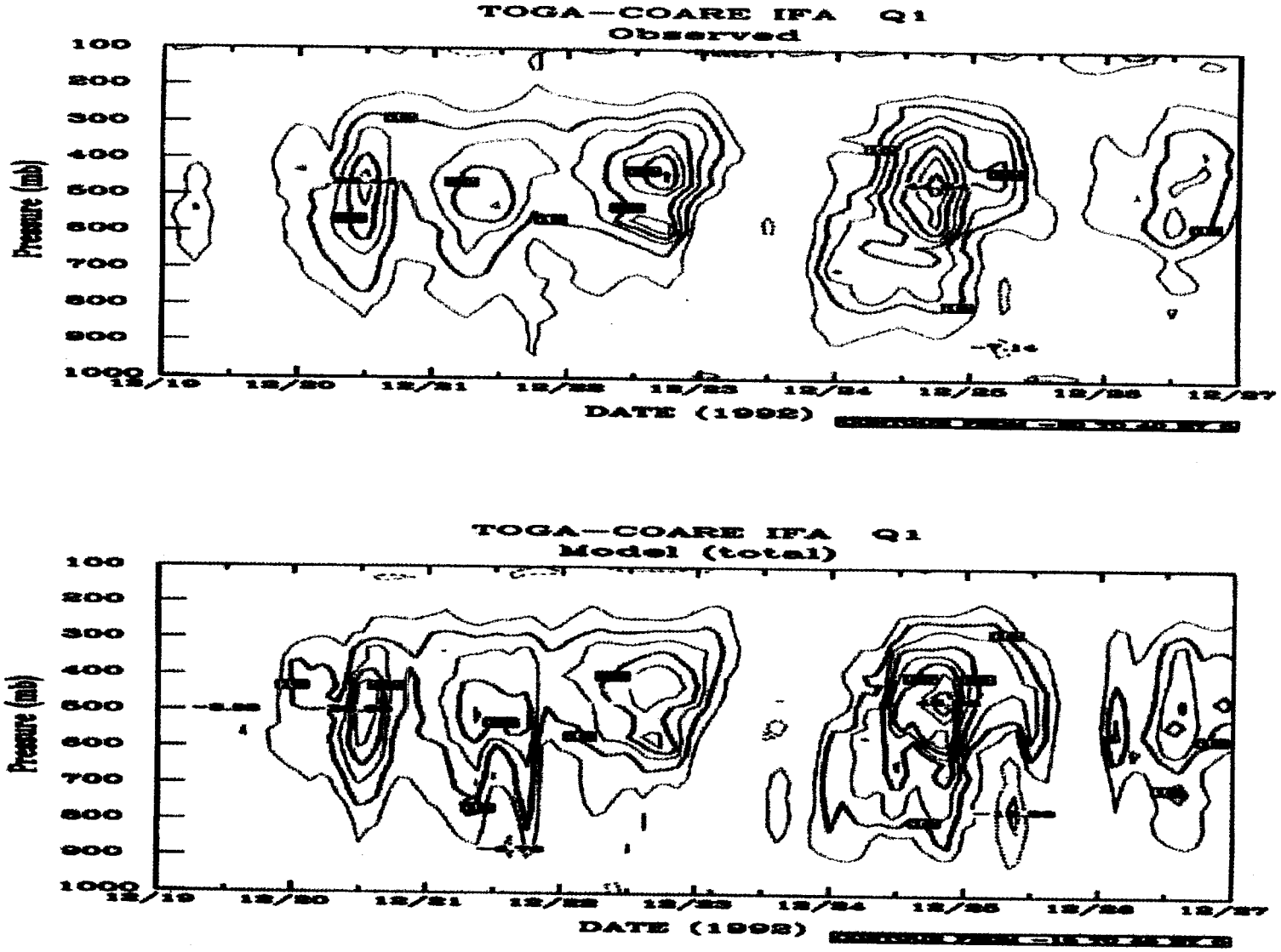
TOGA—COARE IFA Q1
Observed
Pressure (mb)
100
200
300
400
500
600
700
800
900
1000
12/19
12/20
12/21
12/22
12/23
12/24
12/25
12/26
12/27
DATE (1992)
TOGA—COARE IFA Q1
Model (total)
Pressure (mb)
DATE (1992)

Fig. 2

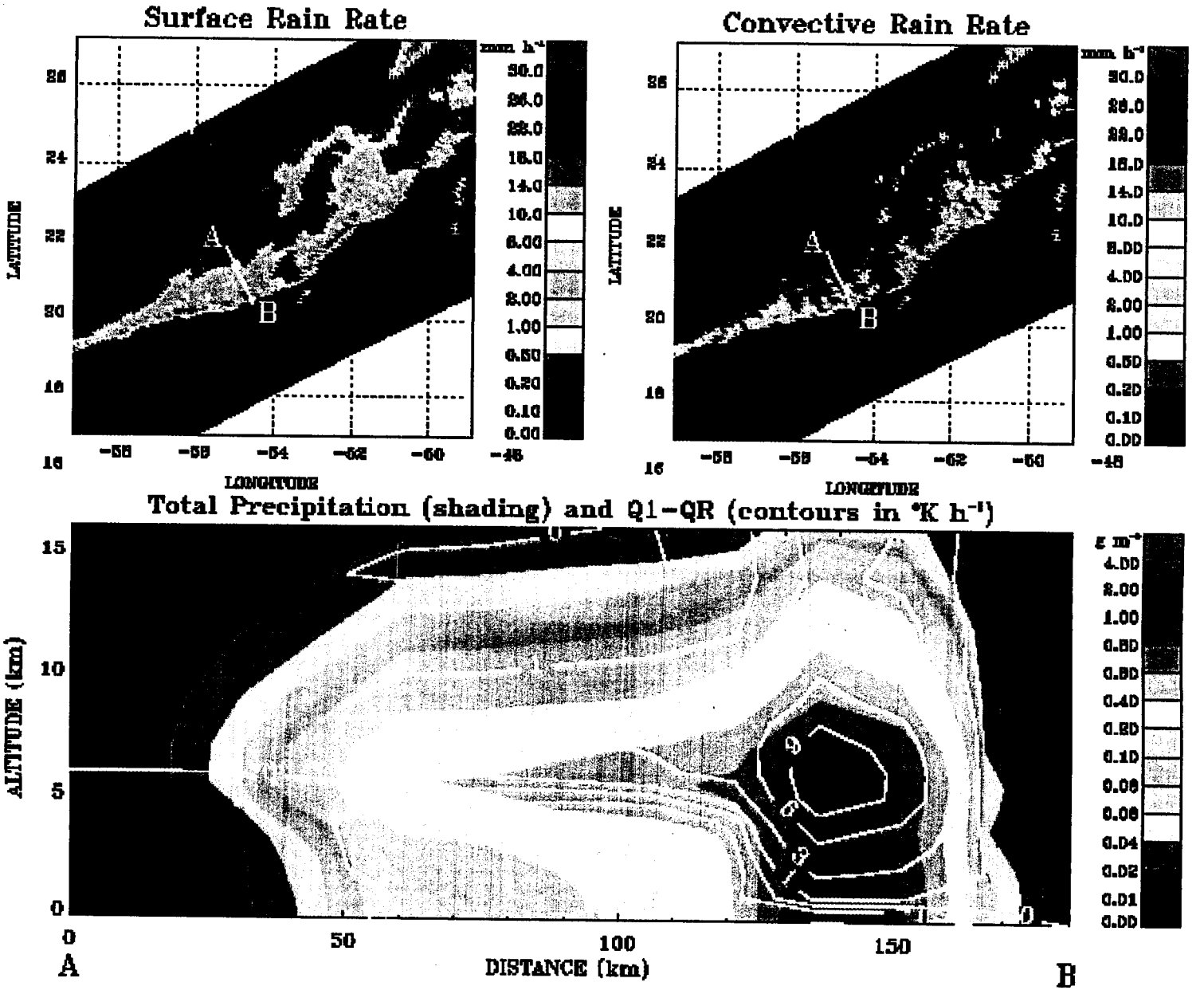
Surface Rain Rate
Convective Rain Rate
LATITUDE
LONGITUDE
A
B
mm h⁻¹
Total Precipitation (shading) and Q1−QR (contours in °K h⁻¹)
ALTITUDE (km)
DISTANCE (km)
0
50
100
150
5
10
15
A
B

Fig. 3

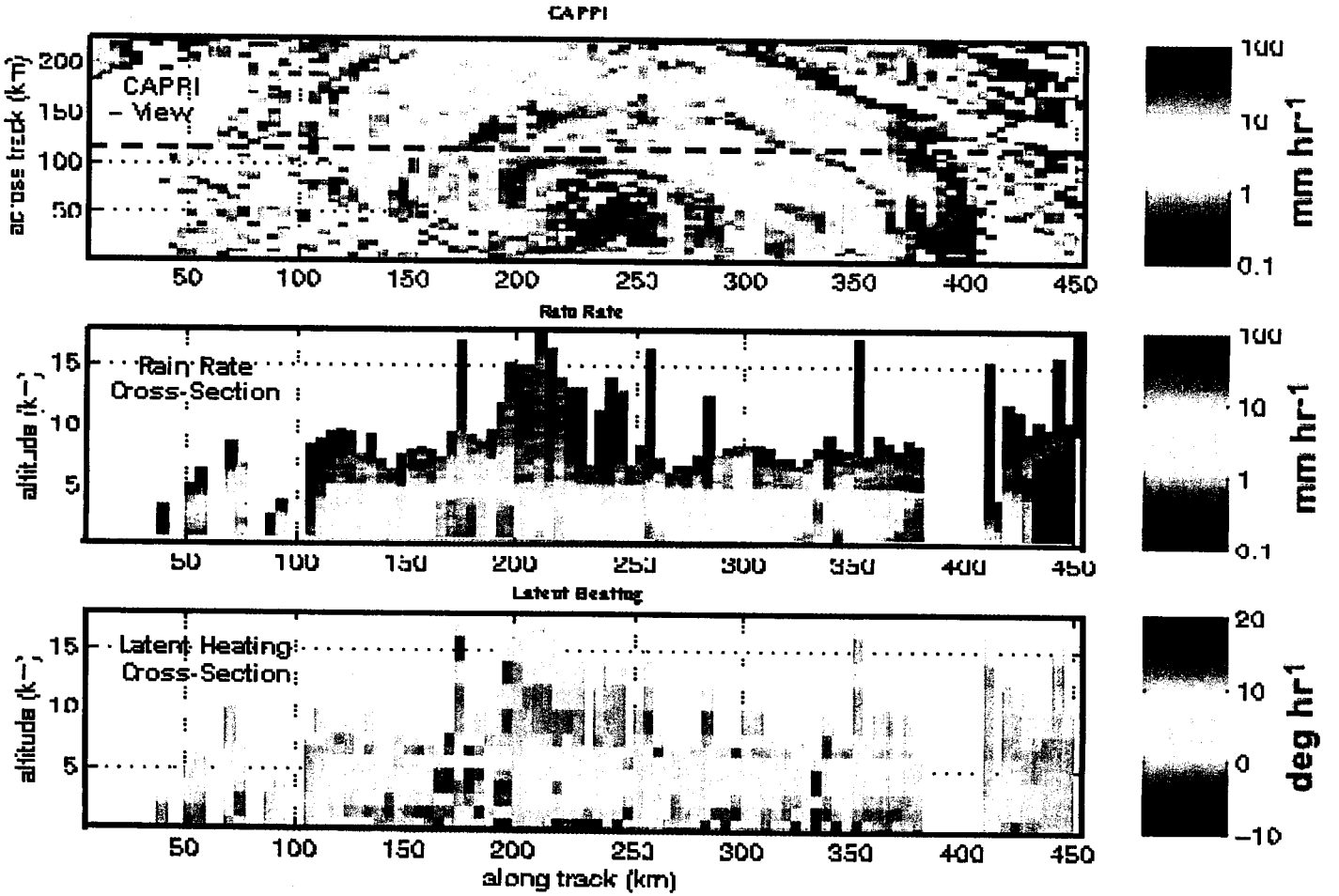
CAPPI
CAPPI
– View
across track (km)
200
150
100
50
50
100
150
200
250
300
350
400
450
100
10
1
0.1
mm hr-1
Rain Rate
Rain Rate
Cross-Section
altitude (km)
15
10
5
50
100
150
200
250
300
350
400
450
100
10
1
0.1
mm hr-1
Latent Heating
Latent Heating
Cross-Section
altitude (km)
15
10
5
50
100
150
200
250
300
350
400
450
along track (km)
20
10
0
–10
deg hr-1

Fig. 4

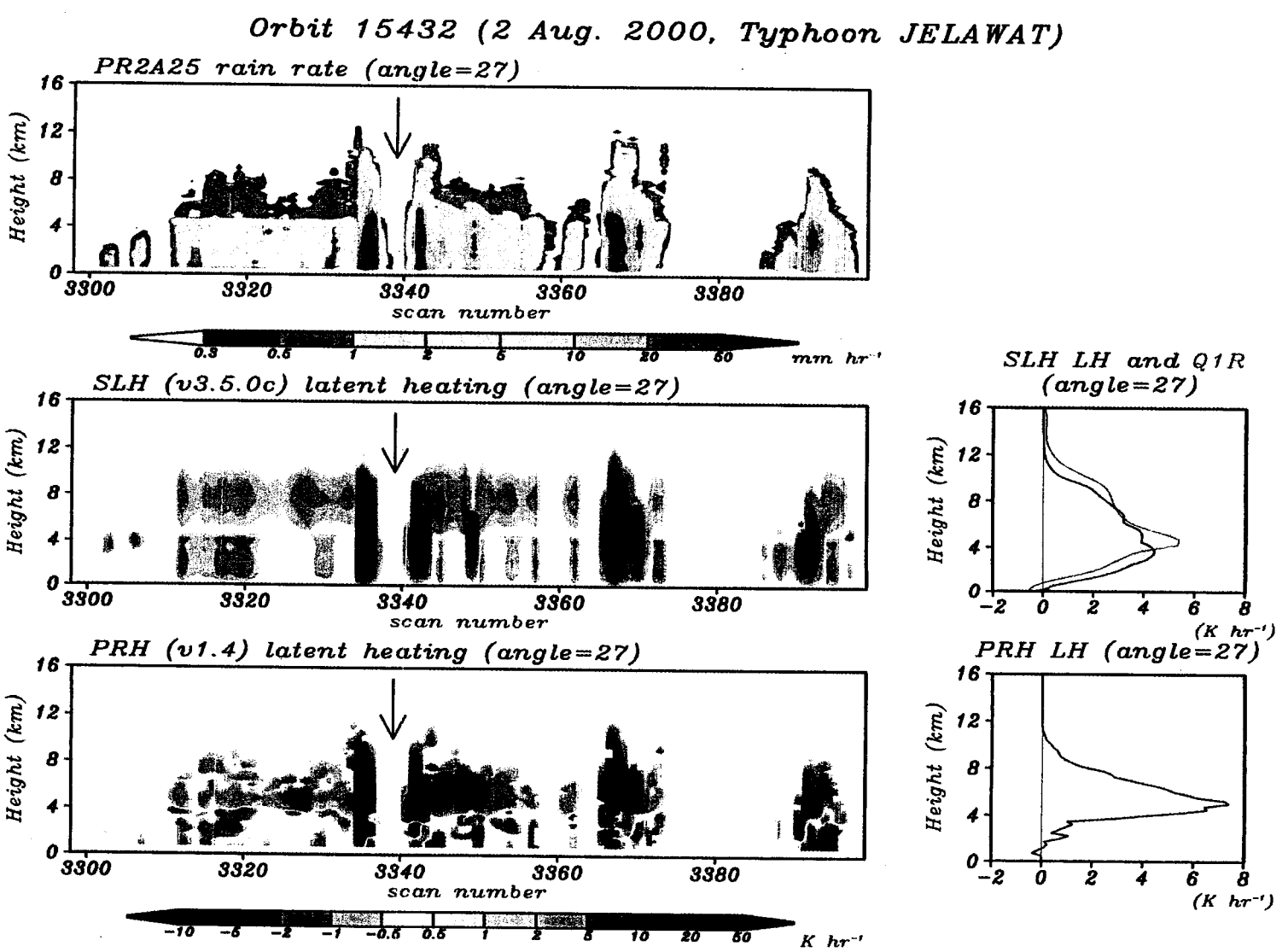
Orbit 15432 (2 Aug. 2000, Typhoon JELAWAT)
PR2A25 rain rate (angle=27)
Height (km)
scan number
mm hr⁻¹
SLH (v3.5.0c) latent heating (angle=27)
PRH (v1.4) latent heating (angle=27)
K hr⁻¹
SLH LH and Q1R (angle=27)
PRH LH (angle=27)
(K hr⁻¹)

Fig. 5

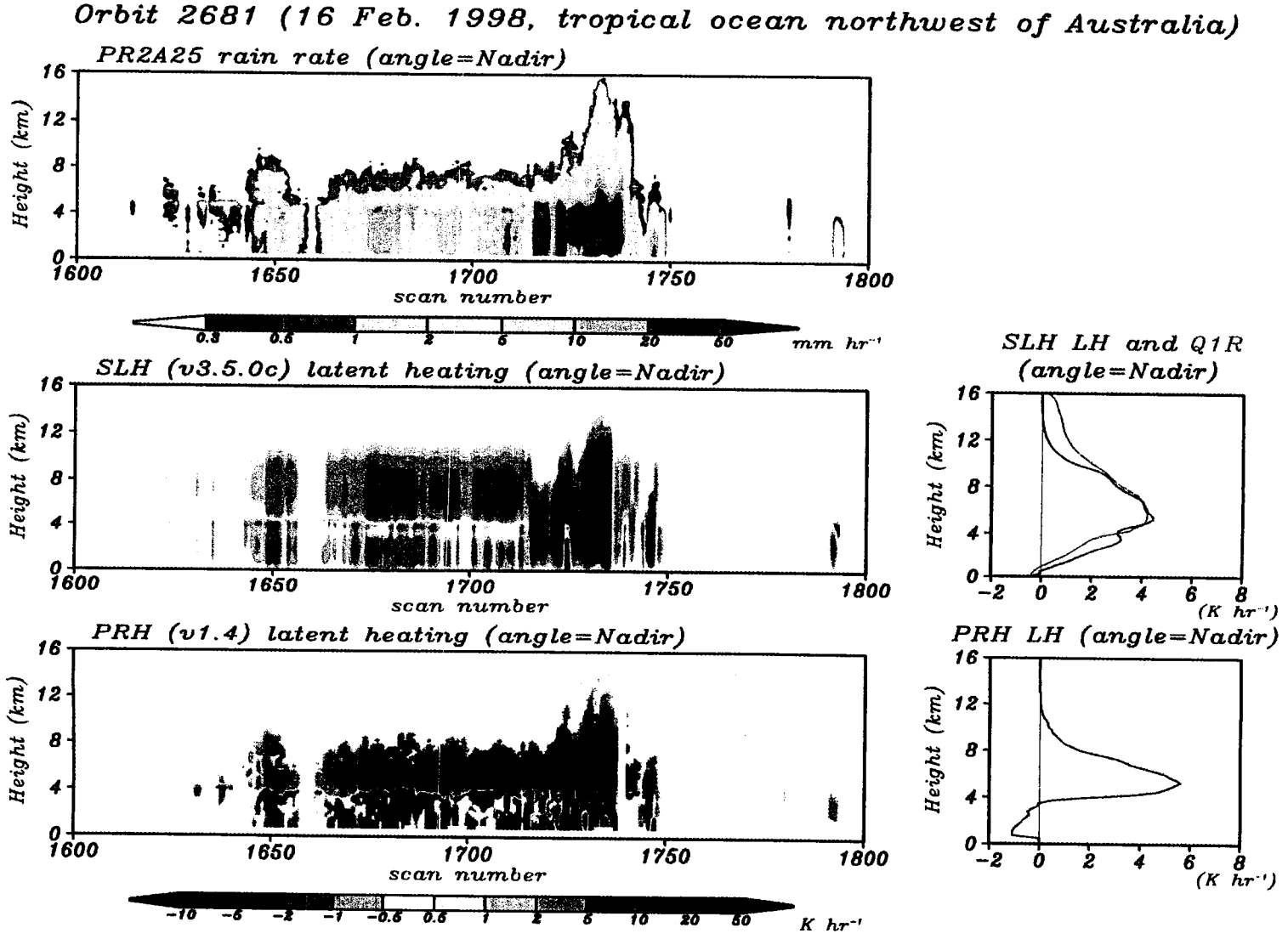
Orbit 2681 (16 Feb. 1998, tropical ocean northwest of Australia)
PR2A25 rain rate (angle=Nadir)
Height (km)
scan number
mm hr⁻¹
SLH (v3.5.0c) latent heating (angle=Nadir)
PRH (v1.4) latent heating (angle=Nadir)
K hr⁻¹
SLH LH and Q1R (angle=Nadir)
PRH LH (angle=Nadir)
(K hr⁻¹)

Fig. 6

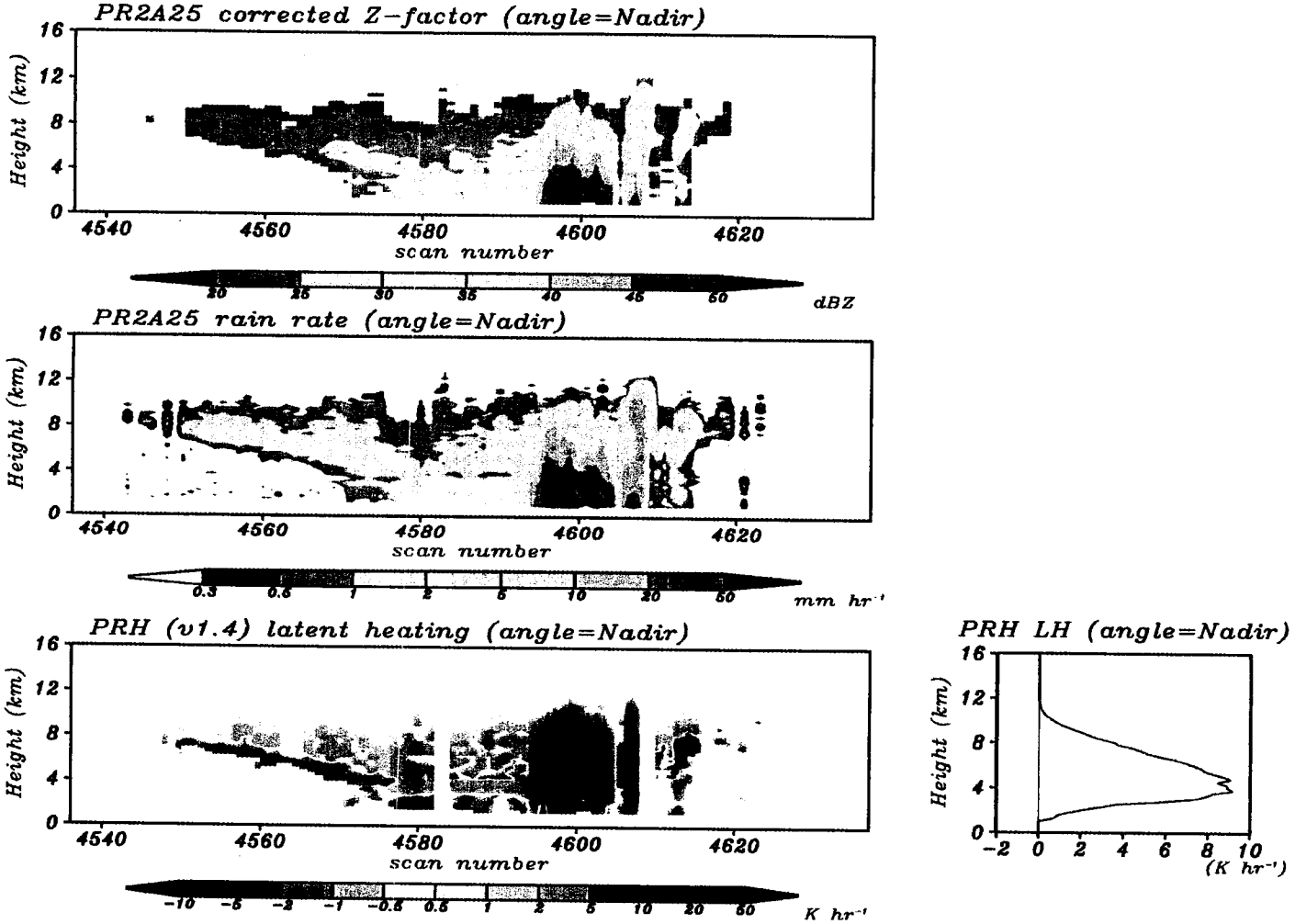
Orbit 8329 (10 May 1999, Oklahoma squall line)
PR2A25 corrected Z-factor (angle=Nadir)
Height (km)
16
12
8
4
0
4540
4560
4580
4600
4620
scan number
20
25
30
35
40
45
60
dBZ
PR2A25 rain rate (angle=Nadir)
Height (km)
scan number
0.3
0.6
1
2
5
10
20
50
mm hr⁻¹
PRH (v1.4) latent heating (angle=Nadir)
Height (km)
scan number
-10
-5
-2
-1
-0.5
0.5
1
2
5
10
20
50
K hr⁻¹
PRH LH (angle=Nadir)
Height (km)
-2
0
2
4
6
8
10
(K hr⁻¹)

Fig. 7

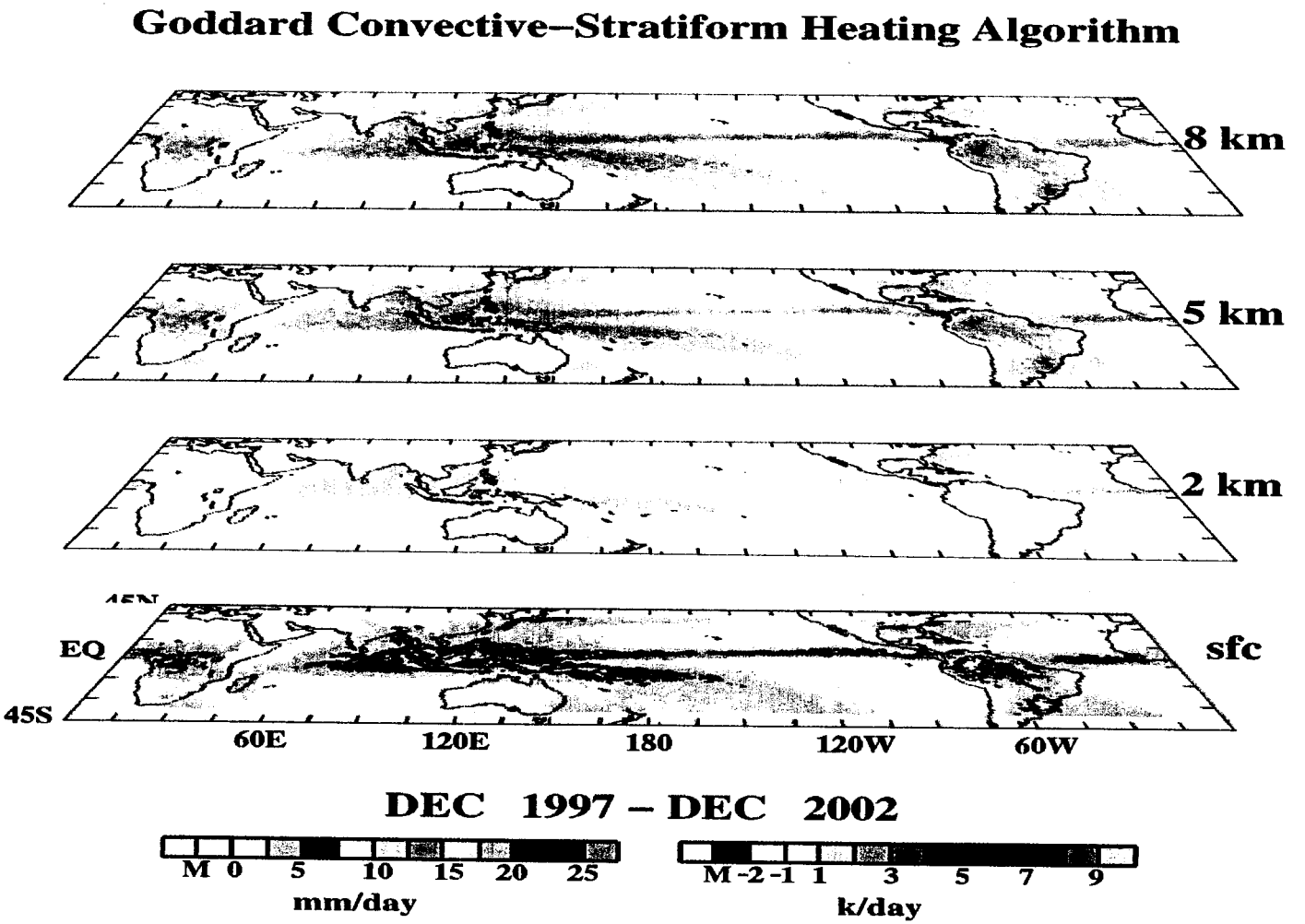
Goddard Convective–Stratiform Heating Algorithm
8 km
5 km
2 km
EQ
sfc
45S
60E
120E
180
120W
60W
DEC 1997 – DEC 2002
M 0 5 10 15 20 25
mm/day
M -2 -1 1 3 5 7 9
k/day

Fig. 8

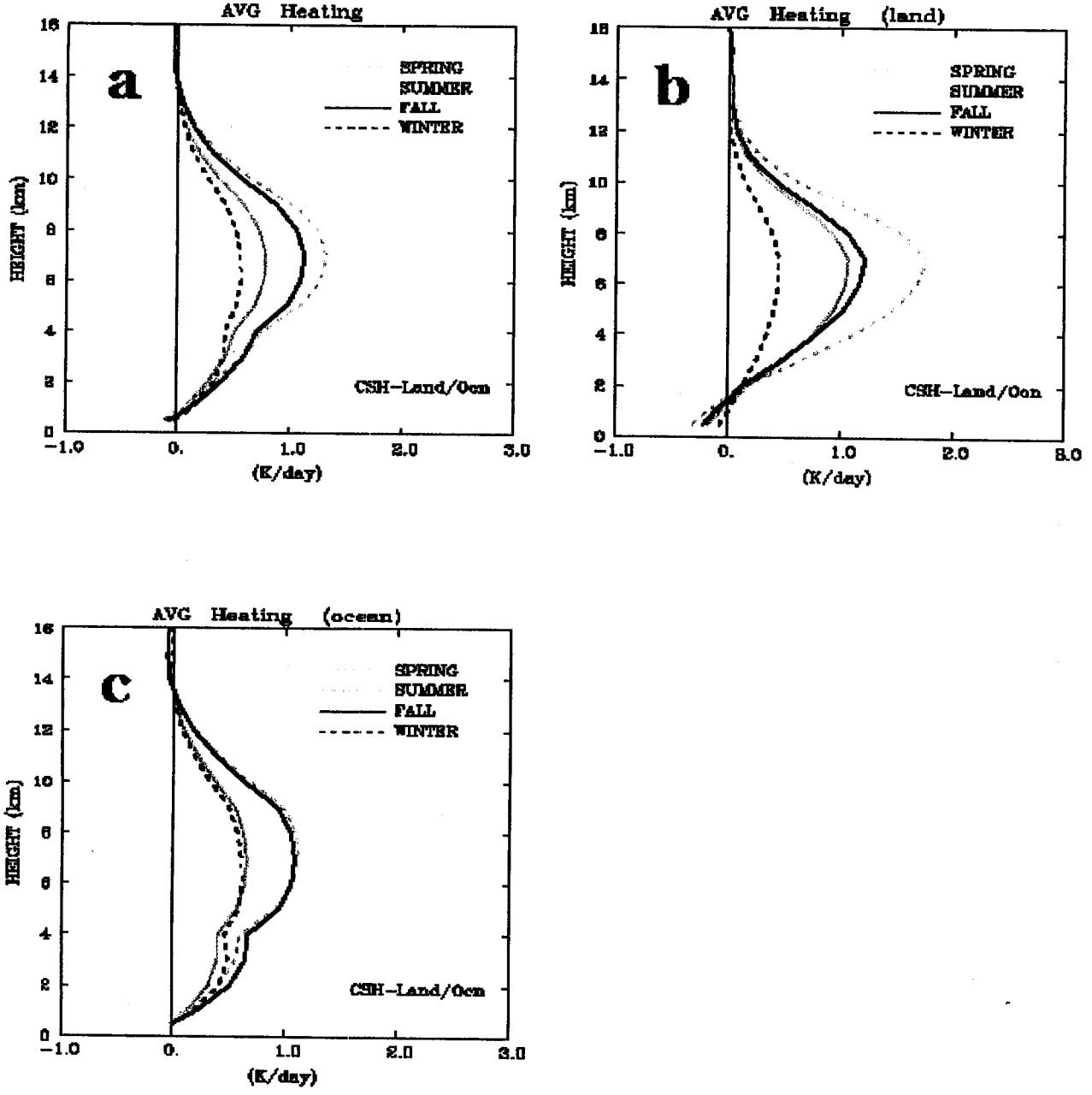
AVG Heating
a
SPRING
SUMMER
FALL
WINTER
CSH-Land/Ocn
HEIGHT (km)
(K/day)
AVG Heating (land)
b
SPRING
SUMMER
FALL
WINTER
CSH-Land/Ocn
HEIGHT (km)
(K/day)
AVG Heating (ocean)
c
SPRING
SUMMER
FALL
WINTER
CSH-Land/Ocn
HEIGHT (km)
(K/day)

Fig. 9

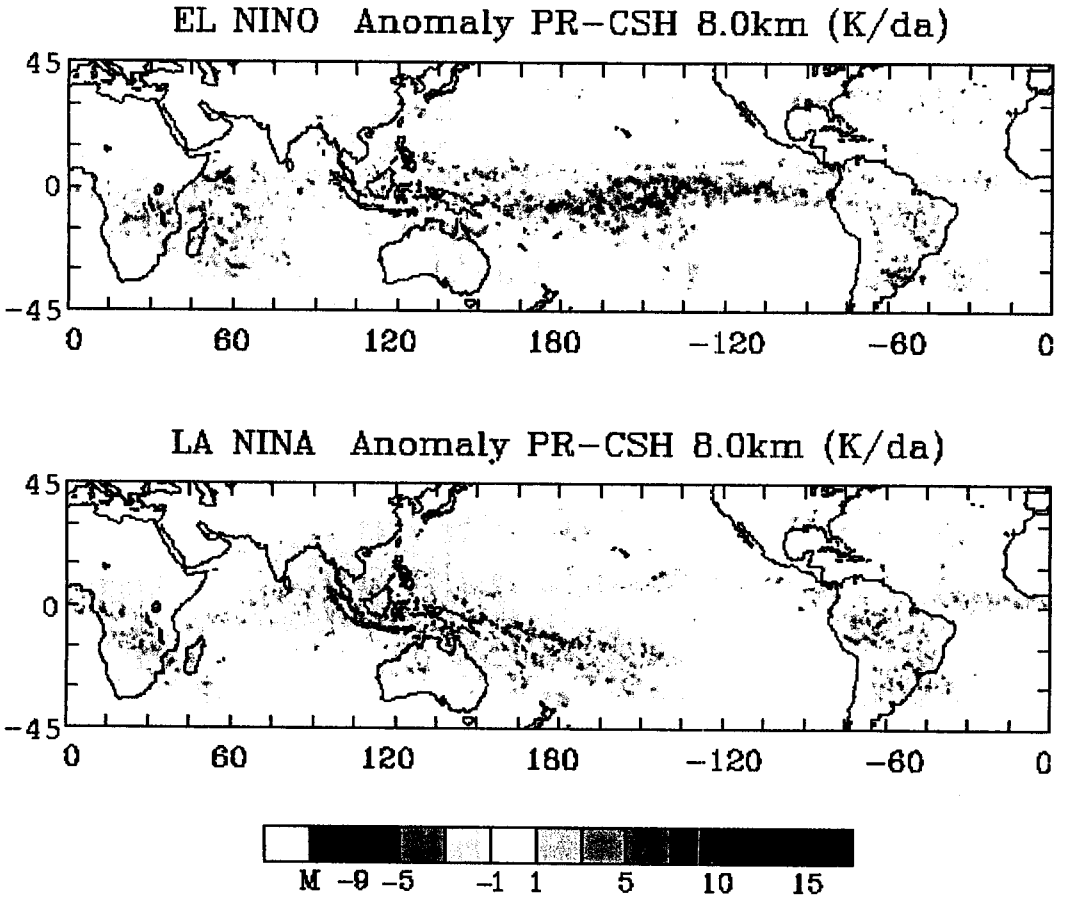
EL NINO Anomaly PR-CSH 8.0km (K/da)
45
0
-45
0
60
120
180
-120
-60
0
LA NINA Anomaly PR-CSH 8.0km (K/da)
45
0
-45
0
60
120
180
-120
-60
0
M -9 -5 -1 1 5 10 15

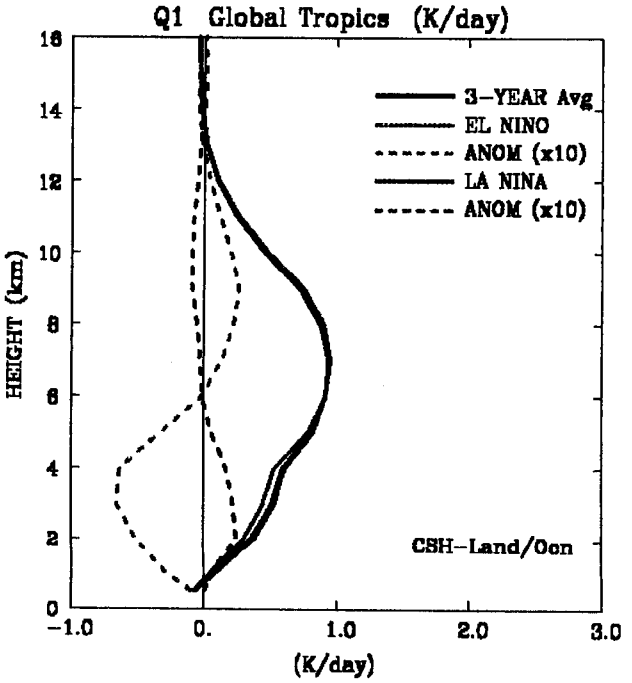
Q1 Global Tropics (K/day)
HEIGHT (km)
16
14
12
10
8
6
4
2
0
-1.0
0.
1.0
2.0
3.0
(K/day)
3-YEAR Avg
EL NINO
ANOM (x10)
LA NINA
ANOM (x10)
CSH-Land/Ocn

Fig. 10

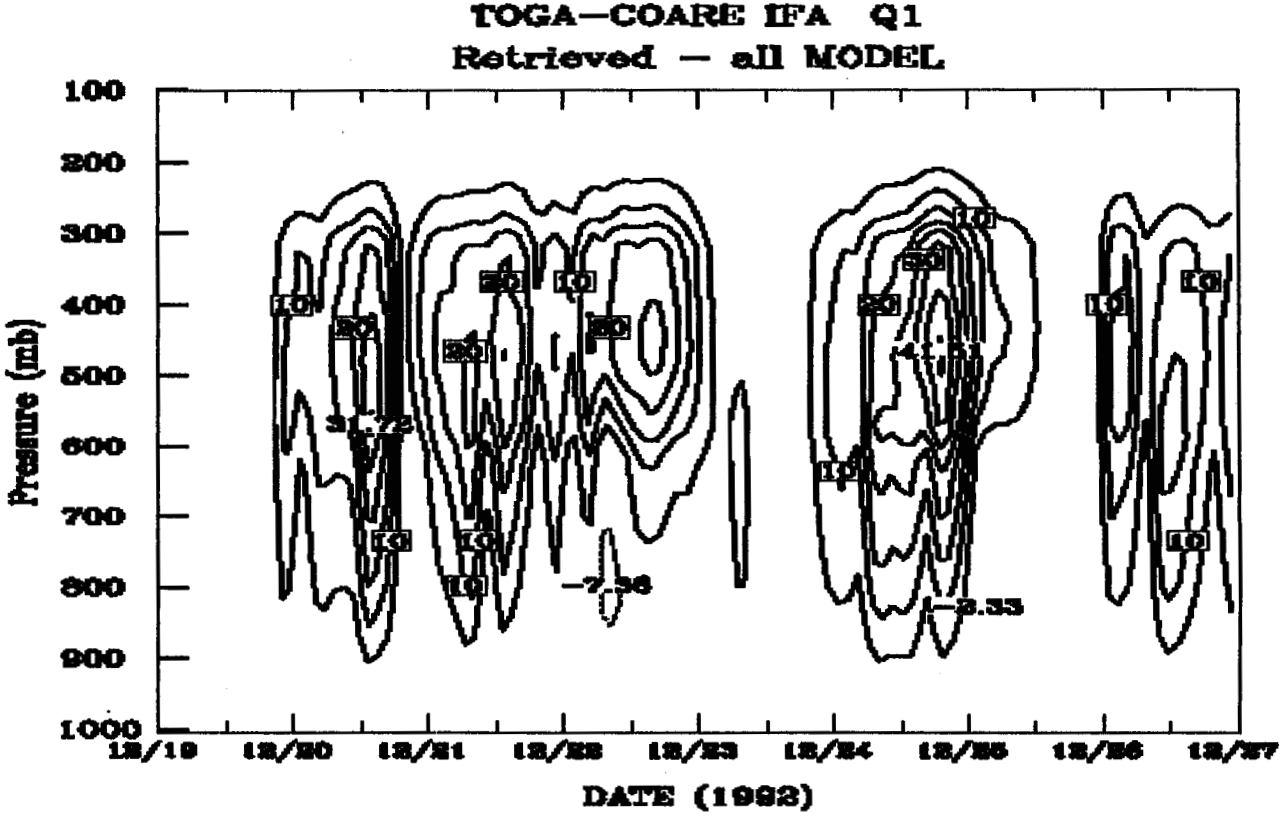
TOGA—COARE IFA Q1
Retrieved — all MODEL
Pressure (mb)
100
200
300
400
500
600
700
800
900
1000
12/19
12/20
12/21
12/22
12/23
12/24
12/25
12/26
12/27
DATE (1992)

Fig. 11

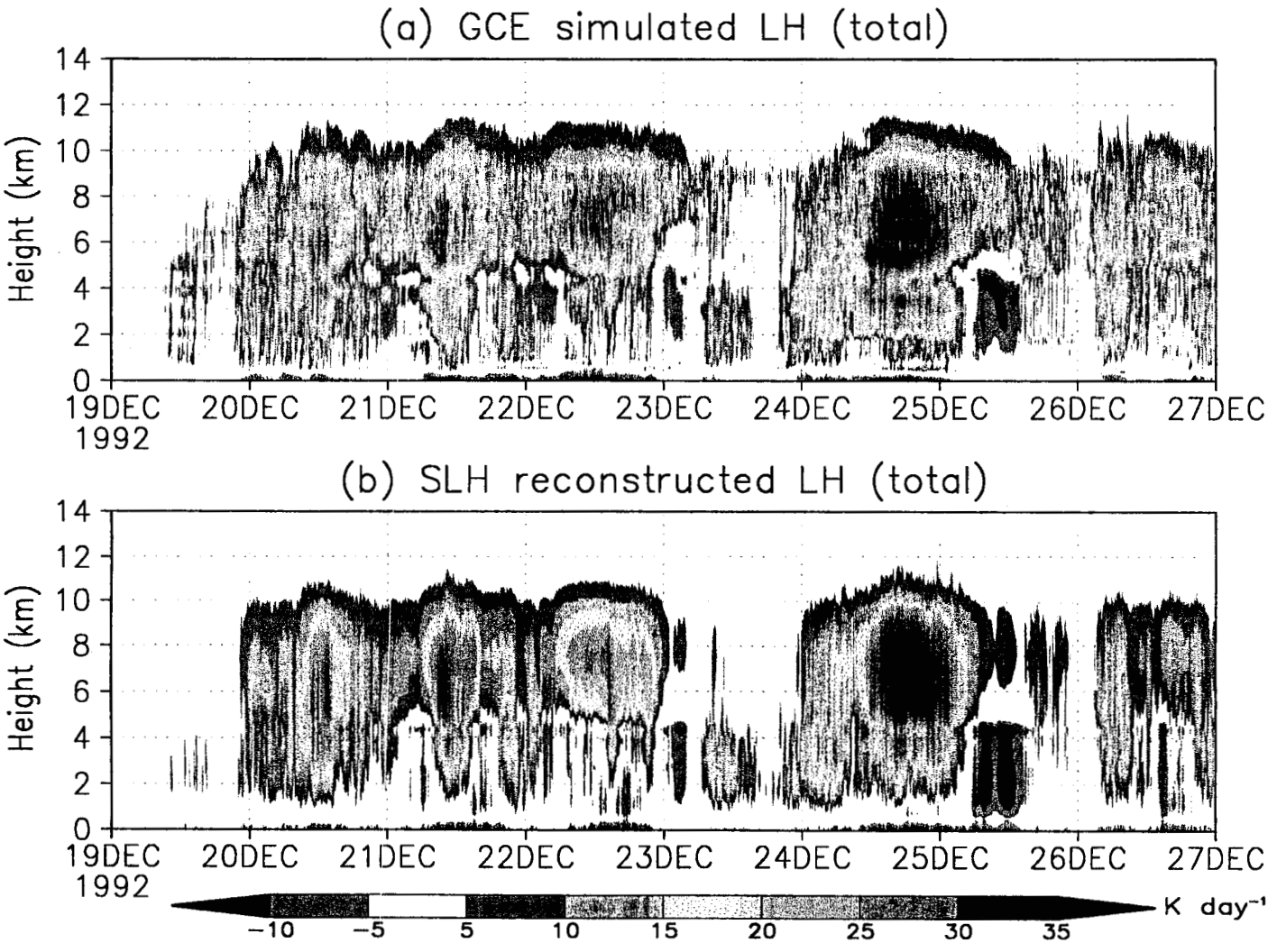
(a) GCE simulated LH (total)
Height (km)
14
12
10
8
6
4
2
0
19DEC
1992
20DEC
21DEC
22DEC
23DEC
24DEC
25DEC
26DEC
27DEC
(b) SLH reconstructed LH (total)
Height (km)
14
12
10
8
6
4
2
0
19DEC
1992
20DEC
21DEC
22DEC
23DEC
24DEC
25DEC
26DEC
27DEC
−10
−5
5
10
15
20
25
30
35
K day⁻¹

Fig. 12

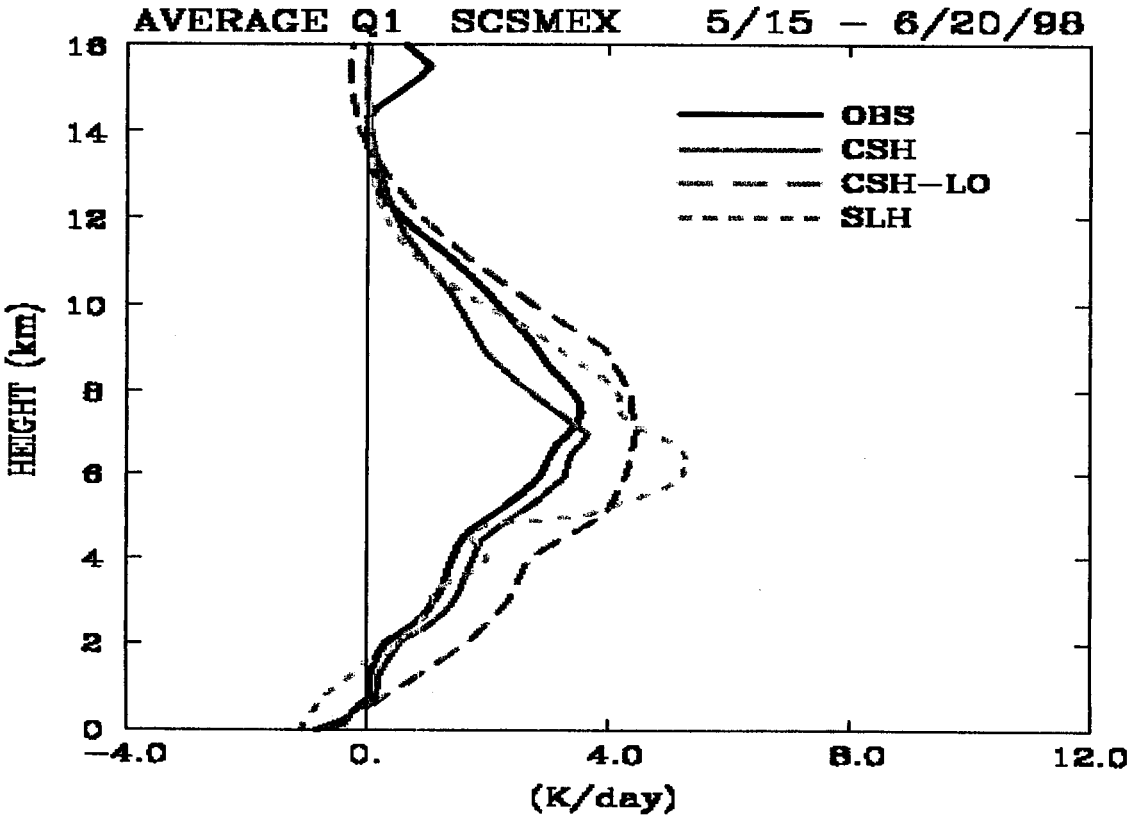
AVERAGE Q1 SCSMEX 5/15 – 6/20/98
OBS
CSH
CSH–LO
SLH
HEIGHT (km)
16
14
12
10
8
6
4
2
0
–4.0
0.
4.0
8.0
12.0
(K/day)

Fig. 13

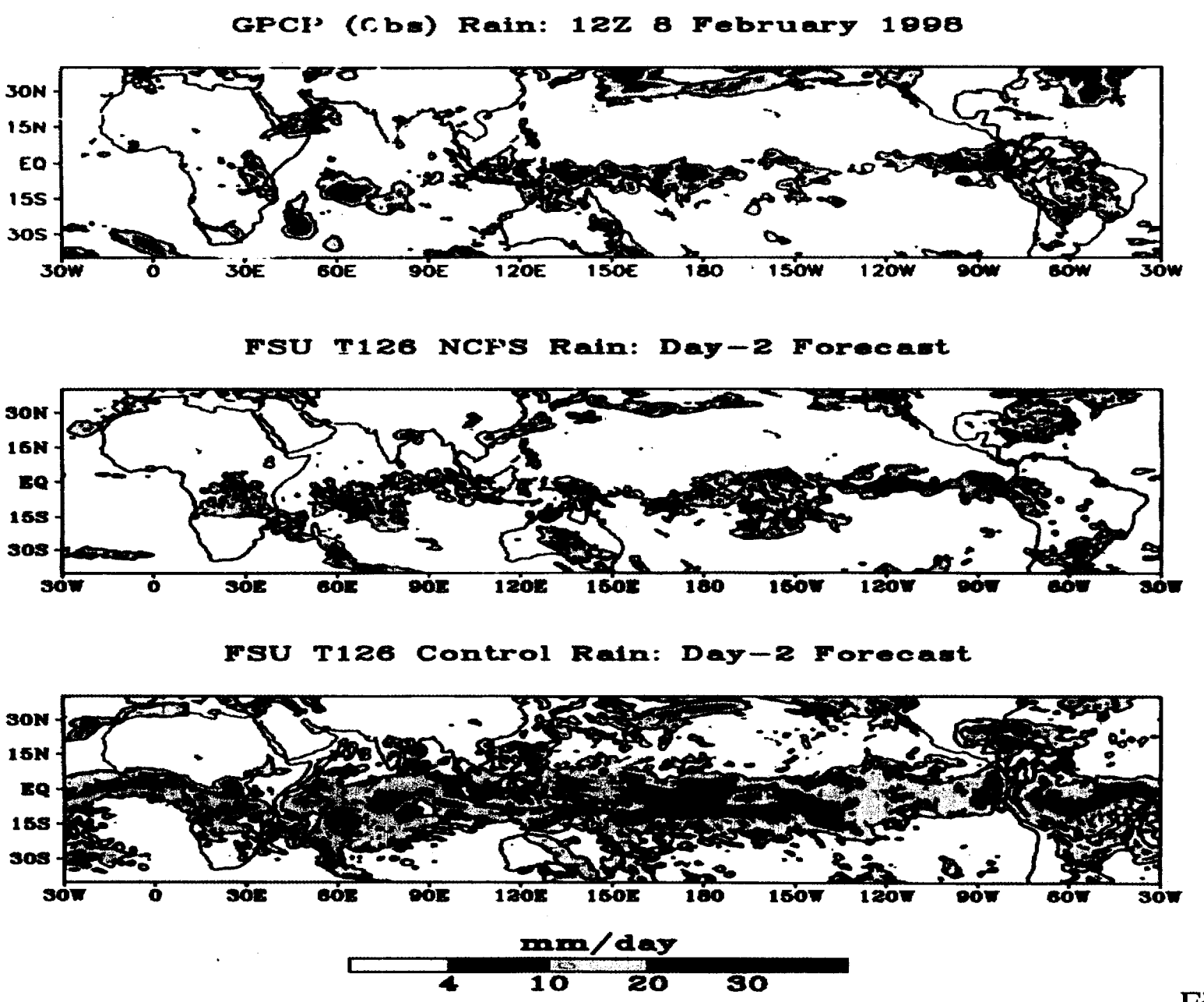
GPCP (Obs) Rain: 12Z 8 February 1998
30N
15N
EQ
15S
30S
30W 0 30E 60E 90E 120E 150E 180 150W 120W 90W 60W 30W
FSU T126 NCEP Rain: Day-2 Forecast
30N
15N
EQ
15S
30S
30W 0 30E 60E 90E 120E 150E 180 150W 120W 90W 60W 30W
FSU T126 Control Rain: Day-2 Forecast
30N
15N
EQ
15S
30S
30W 0 30E 60E 90E 120E 150E 180 150W 120W 90W 60W 30W
mm/day
4 10 20 30

Fig. 14